Supplementary Information for

Structural Variation, Magnetism and Single-source Deposition of Lanthanide-containing Polyoxotitanates

Rosa Müller,[a] Olivia Georghiades,[a] Joshua D. Bocarsly,[a] Farheen N. Sayed,[a] Victor Riesgo Gonzalez,[a] Andrew D. Bond,[a] Clare P. Grey[a] and Dominic S. Wright*[,a]

[a] The Yusuf Hamied Department of Chemistry, Cambridge University, Lensfield Road, Cambridge CB2 1EW, UK. E-mail: dsw1000@cam.ac.uk; Tel: +44 (0)1223 763122.

Synthesis of Ln-POTs

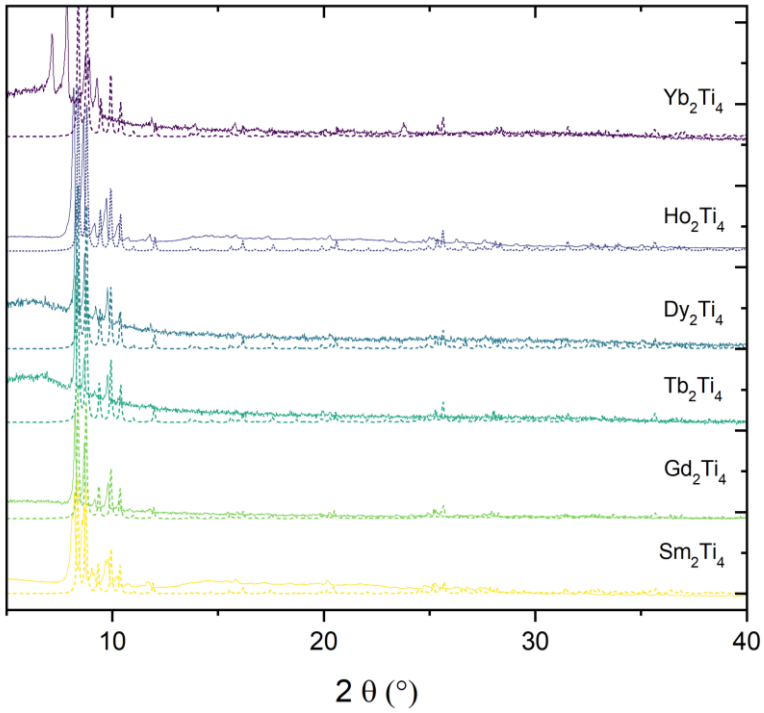

Figure S1 Experimental powder diffraction patterns of the newly synthesised Ln_2Ti_4-cages (Ln = Sm, Gd, Tb, Dy, Ho, Yb) and their predicted patterns (dashed line) calculated from the single crystal data. Some impurities in form of $Ti_{16}O_{16}(OEt)_{32}$, indicated by low-angle diffraction peaks are present in case of **Yb_2Ti_4**. For **Tm_2Ti_4** not enough sample for bulk analysis was obtained.

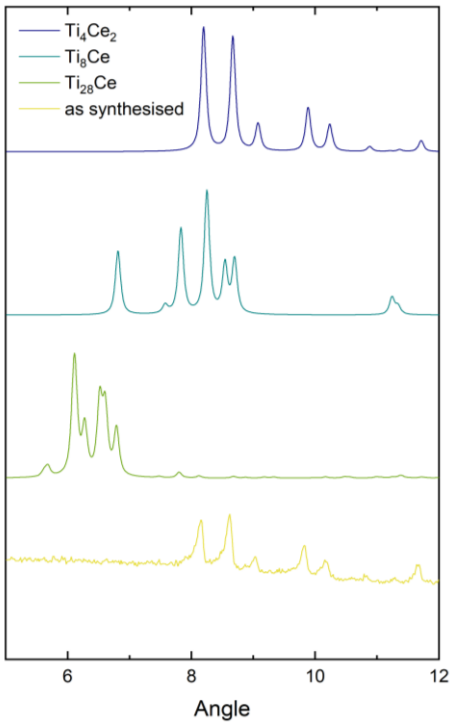

Figure S2 Comparison of the experimental powder diffraction data obtained for the synthesised Ce-POTs with calculated diffraction patterns of the possible reaction products **$Ti_{28}Ce$**, **Ti_8Ce** and **Ti_4Ce_2**. The smallest cage type **Ti_4Ce_2** is found to be the main component.

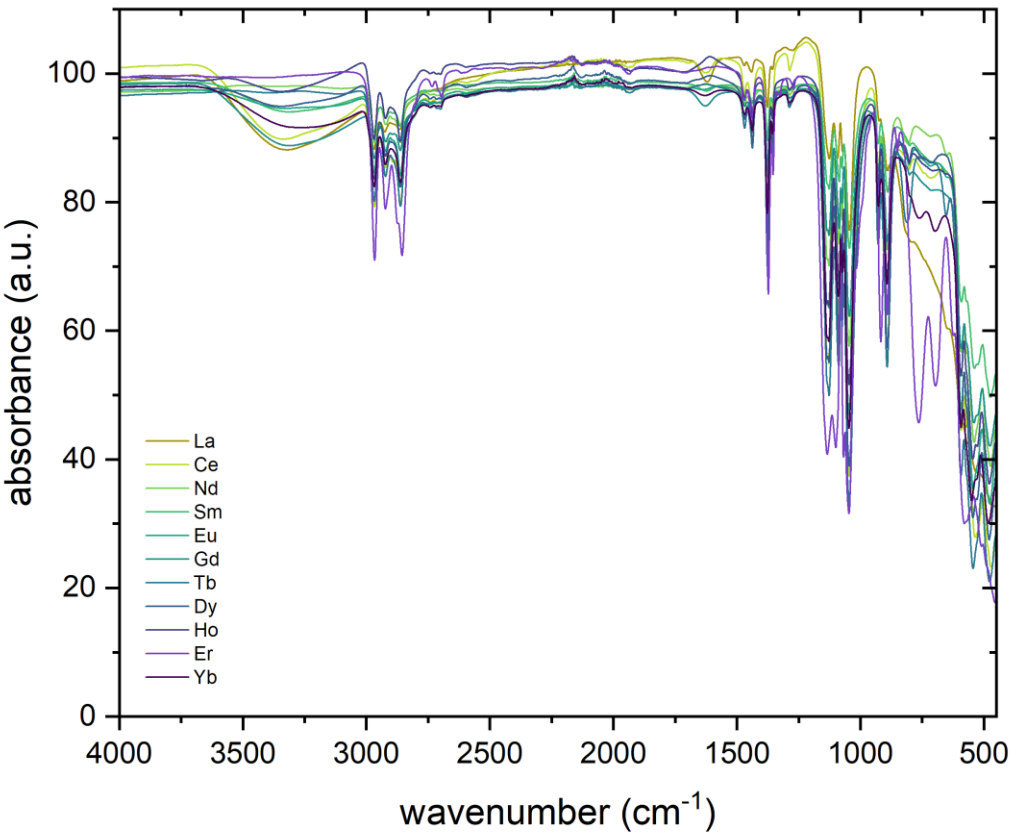

Figure S3 IR spectra of the complete series of Ln-POTs (Ln = La-Er, Yb). Not enough sample was obtained in case of Ln = Tm. A distinct spectrum is observed for Ln = Er (**Ti_8Er**).

Crystallographic data

Table S1 Crystallographic and refinement data for Ti_4Ln_2 (Ln = Sm, Gd, Tb, Dy, Ho, Er, Tm, Yb).

	Ti_4Sm_2	**Ti_4Gd_2**	**Ti_4Tb_2**	**Ti_4Dy_2**	**Ti_4Ho_2**	**Ti_4Er_2**	**Ti_4Tm_2**	**Ti_4Yb_2**
CCDC number	2283720	2283721	2283722	2283715	2283717	2283719	2283718	2283716
Cambridge data number	DW_B1_0414	DW_B2_0373	DW_B1_0430	DW_B2_0375	DW_B1_0431	DW_B1_0463	DW_B1_0479	DW_B1_0396
Chemical formula	$C_{36}H_{92}Cl_2O_{20}Sm_2Ti_4$	$C_{36}H_{92}Cl_2O_{20}Gd_2Ti_4$	$C_{36}H_{92}Cl_2O_{20}Tb_2Ti_4$	$C_{36}H_{92}Cl_2O_{20}Dy_2Ti_4$	$C_{36}H_{92}Cl_2O_{20}Ho_2Ti_4$	$C_{36}H_{92}Cl_2O_{20}Er_2Ti_4$	$C_{36}H_{92}Cl_2O_{20}Tm_2Ti_4$	$C_{36}H_{92}Cl_2O_{20}Yb_2Ti_4$
Formula weight	1408.29	1422.09	1425.43	1432.59	1437.45	1442.11	1445.45	1453.67
Temperature / K	180(2)	180(2)	180(2)	180(2)	180(2)	180(2)	180(2)	180(2)
Crystal system	monoclinic	monoclinic	monoclinic	monoclinic	monoclinic	monoclinic	monoclinic	monoclinic
Space group	P $2_1/n$	P $2_1/n$	P $2_1/n$	P $2_1/n$	P $2_1/n$	P $2_1/n$	P $2_1/n$	P $2_1/n$
a / Å	11.9374(4)	11.9414(5)	11.9091(5)	11.9219(5)	11.9118(4)	11.9203(6)	11.9196(4)	11.9050(3)
b / Å	18.9359(6)	18.8718(8)	18.8221(8)	18.7644(8)	18.7283(6)	18.7662(10)	18.7621(6)	18.6786(5)
c / Å	12.7346(4)	12.7327(5)	12.7415(6)	12.7482(6)	12.7532(4)	12.7290(7)	12.7550(4)	12.7568(4)
alpha / °	90	90	90	90	90	90	90	90
beta / °	92.3995(12)	92.454(2)	92.592(2)	92.549(2)	92.6111(12)	92.705(3)	92.8718(13)	92.6397(11)
gamma / °	90	90	90	90	90	90	90	90
Unit-cell volume / $Å^3$	2876.07(16)	2866.8(2)	2853.1(2)	2849.0(2)	2842.13(16)	2844.3(3)	2848.90(16)	2833.70(14)
Z	2	2	2	2	2	2	2	2
Calc. density / g cm^{-3}	1.626	1.647	1.659	1.670	1.680	1.684	1.685	1.704
F(000)	1428	1436	1440	1444	1448	1452	1456	1460
Radiation type	Cu K	Cu K	Cu K	Cu K	Cu K	Cu K	Cu K	Cu K
Absorption coefficient / mm^{-1}	20.963	20.613	17.865	19.716	10.897	11.170	11.517	11.819
Crystal size / mm^3	0.16 x 0.16 x 0.08	0.10 x 0.10 x 0.08	0.12 x 0.10 x 0.10	0.08 x 0.08 x 0.04	0.10 x 0.10 x 0.08	0.16 x 0.10 x 0.06	0.15 x 0.10 x 0.10	0.14 x 0.14 x 0.12
2 range / °	10.99–133.26	9.37–133.59	11.00–133.28	11.00–133.06	9.44–133.20	8.40–133.41	10.98–133.30	8.40–133.63
Completeness to max 2	0.994	0.993	0.992	0.995	0.992	0.998	0.994	0.999
No. of reflections measured	28827	49395	41828	28283	31868	40698	47040	46776
No. of independent reflections	5059	5049	5005	5003	4981	5024	5004	5020
R(int)	0.0364	0.0435	0.0433	0.0435	0.0312	0.1390	0.0410	0.0500
No. parameters / restraints	329 / 60	329 / 60	329 / 60	329 / 12	329 / 60	309 / 144	318 / 143	338 / 60
Final R1 values (I > 2(I))	0.0212	0.0183	0.0212	0.0210	0.0206	0.0532	0.0200	0.0244
Final wR(F^2) values (all data)	0.0531	0.0448	0.0526	0.0490	0.0505	0.1478	0.0511	0.0591
Goodness-of-fit on F^2	1.047	1.050	1.066	1.043	1.076	1.023	1.071	1.081
Largest diff. peak & hole / e $Å^{-3}$	0.601, –0.802	0.331, –0.576	0.471, –0.702	0.307, –0.410	0.319, –0.545	2.495, –1.245	0.545, –0.917	1.356, –0.882

Analysis of the TiO_6 octahedral geometry

Table S2 Continuous Shape Measure (CShM, implemented at: https://csm.ouproj.org.il/molecule [I. Tuvi-Arad, G. Alon and D. Avnir]) for Ti_4Ln_2 cages, quantifying the distortion of the TiO_6 octahedra from regularity. The TiO_6 octahedra were isolated from each structure and compared to a regular octahedron with a central point (7-point comparison). CShM = 0 indicates a regular octahedron. Increasing CShM indicates increasing distortion from the regular octahedron.

	Ti_4Ce_2 ZIWYEM	Ti_4Nd_2 DEJRIV	Ti_4Sm_2	Ti_4Eu_2 CURJEG	Ti_4Gd_2	Ti_4Tb_2	Ti_4Dy_2	Ti_4Ho_2	Ti_4Er_2	Ti_4Tm_2	Ti_4Yb_2
Ti1—O1	1.934	1.936	1.9371(17)	1.936	1.9357(15)	1.9338(15)	1.9328(18)	1.9348(13)	1.922(5)	1.9312(16)	1.931(2)
Ti1—O2	2.067	2.072	2.0639(17)	2.071	2.0642(15)	2.0617(16)	2.0635(18)	2.0643(13)	2.051(5)	2.0620(16)	2.056(2)
Ti1—O4	2.178	2.183	2.1690(17)	2.168	2.1674(15)	2.1593(15)	2.1583(16)	2.1554(13)	2.158(5)	2.1482(16)	2.145(2)
Ti1—O5	1.777	1.789	1.7888(18)	1.789	1.7902(15)	1.7890(16)	1.7880(17)	1.7866(14)	1.795(5)	1.7884(17)	1.786(2)
Ti1—O6	1.859	1.859	1.8649(18)	1.861	1.8622(15)	1.8578(15)	1.8582(16)	1.8600(13)	1.845(5)	1.8562(16)	1.856(2)
Ti1—O10	1.987	1.977	1.9774(17)	1.981	1.9773(14)	1.9819(15)	1.9833(16)	1.9827(12)	1.982(5)	1.9890(15)	1.992(2)
O5—Ti1—O6	98.12	98.99	98.86(8)	98.51	98.78(7)	98.73(7)	98.68(8)	98.65(6)	97.9(2)	98.30(8)	98.54(11)
O5—Ti1—O1	99.30	99.14	99.09(8)	99.05	99.10(7)	99.28(7)	99.27(8)	99.38(6)	99.1(3)	99.48(8)	99.43(11)
O6—Ti1—O1	102.61	103.08	103.34(8)	103.62	103.75(7)	103.86(7)	104.17(8)	104.07(6)	104.0(2)	104.09(7)	104.41(10)
O5—Ti1—O10	164.07	163.24	163.70(8)	164.05	163.82(7)	164.14(7)	164.25(8)	164.33(6)	164.3(3)	164.51(8)	164.78(10)
O6—Ti1—O10	96.29	96.47	96.33(7)	96.41	96.37(6)	96.12(6)	96.12(7)	96.12(5)	97.0(2)	96.39(7)	95.97(9)
O1—Ti1—O10	84.07	83.52	83.04(7)	82.80	82.73(6)	82.44(6)	82.18(7)	81.98(5)	82.1(2)	81.60(6)	81.27(9)
O5—Ti1—O2	95.77	96.04	96.21(8)	96.41	96.35(7)	96.47(7)	96.61(8)	96.66(6)	97.3(3)	96.93(8)	97.09(11)
O6—Ti1—O2	95.17	94.71	94.79(8)	94.49	94.58(7)	94.48(7)	94.24(8)	94.26(6)	94.8(2)	94.31(7)	94.14(10)
O1—Ti1—O2	154.72	154.40	154.06(7)	154.06	153.82(6)	153.59(6)	153.45(7)	153.42(5)	153.0(2)	153.18(7)	152.91(9)
O10—Ti1—O2	76.17	76.23	76.59(7)	76.78	76.72(6)	76.79(6)	76.91(7)	77.00(5)	76.5(2)	77.03(6)	77.26(9)
O5—Ti1—O4	93.72	92.99	93.20(8)	93.46	93.29(7)	93.58(7)	93.63(7)	93.65(6)	93.8(2)	93.91(7)	93.91(10)
O6—Ti1—O4	165.69	165.35	165.21(7)	165.11	165.06(6)	164.72(6)	164.52(7)	164.58(6)	165.3(2)	164.71(7)	164.26(9)
O1—Ti1—O4	83.26	83.14	83.02(7)	83.07	82.86(6)	82.90(6)	82.90(7)	82.91(5)	82.7(2)	82.80(6)	82.84(9)
O10—Ti1—O4	71.10	70.81	70.93(6)	70.96	70.90(5)	70.90(6)	70.90(6)	70.95(5)	70.7(2)	70.82(6)	71.02(8)
O2—Ti1—O4	75.59	75.57	75.31(7)	75.30	75.24(6)	75.05(6)	74.96(7)	75.01(5)	74.9(2)	75.03(6)	74.72(9)
CShM (Oct)	**1.037**	**1.073**	**1.088**	**1.090**	**1.104**	**1.109**	**1.122**	**1.125**	**1.152**	**1.139**	**1.145**

Table S3 Continuous Shape Measure (CShM), cont'd. Atoms O8 and O10 form the edge bridged by Ln^{3+}: the highlighted O8—Ti2—O10 angle decreases steadily as Ln^{3+} gets smaller across the row (atom numbering in Figure S3). This indicates an increase in structural strain along the series of **Ti_4Ln_2** cages.

	Ti_4Ce_2 ZIWYEM	Ti_4Nd_2 DEJRIV	Ti_4Sm_2	Ti_4Eu_2 CURJEG	Ti_4Gd_2	Ti_4Tb_2	Ti_4Dy_2	Ti_4Ho_2	Ti_4Er_2	Ti_4Tm_2	Ti_4Yb_2
Ti2—O2	2.020	2.024	2.0180(17)	2.023	2.0187(15)	2.0173(15)	2.0185(17)	2.0150(13)	2.005(5)	2.0168(16)	2.015(2)
Ti2—O3	1.919	1.918	1.9195(17)	1.922	1.9214(15)	1.9181(15)	1.9155(17)	1.9173(13)	1.912(5)	1.9155(16)	1.913(2)
Ti2—O4	2.113	2.113	2.1165(17)	2.114	2.1155(14)	2.1150(15)	2.1141(17)	2.1113(13)	2.104(5)	2.1128(16)	2.108(2)
Ti2—O7	1.791	1.789	1.7877(18)	1.790	1.7911(16)	1.7895(16)	1.7884(18)	1.7912(13)	1.790(6)	1.7913(17)	1.792(2)
Ti2—O8	1.914	1.916	1.9135(18)	1.919	1.9169(15)	1.9143(16)	1.9150(17)	1.9162(13)	1.912(5)	1.9155(16)	1.913(2)
Ti2—O10	2.003	1.998	2.0018(16)	2.008	2.0018(14)	2.0020(15)	2.0033(17)	2.0037(12)	1.990(5)	2.0017(16)	2.005(2)
O7—Ti2—O8	101.56	102.42	102.63(8)	102.37	102.77(7)	102.93(7)	102.87(8)	102.87(6)	103.0(2)	103.04(7)	103.01(10)
O7—Ti2—O3	100.72	100.96	101.06(8)	101.00	100.92(7)	101.05(7)	101.06(8)	101.15(6)	101.3(2)	101.29(7)	101.39(10)
O8—Ti2—O3	95.51	95.86	96.39(8)	96.46	96.63(7)	96.82(7)	97.26(7)	97.32(6)	96.6(2)	97.46(7)	97.86(10)
O7—Ti2—O10	169.94	169.37	169.48(8)	169.81	169.74(6)	169.75(7)	169.88(7)	170.12(6)	170.4(2)	170.30(7)	170.33(10)
O8—Ti2—O10	**84.62**	**84.25**	**83.88(7)**	**83.71**	**83.40(6)**	**83.22(6)**	**82.95(7)**	**82.71(5)**	**82.3(2)**	**82.39(6)**	**82.04(9)**
O3—Ti2—O10	86.43	86.40	86.24(7)	86.27	86.32(6)	86.17(6)	86.23(7)	86.03(5)	85.9(2)	85.79(6)	85.90(9)
O7—Ti2—O2	94.19	93.80	93.53(8)	93.52	93.51(7)	93.35(7)	93.21(8)	93.22(6)	93.7(2)	93.22(7)	93.01(10)
O8—Ti2—O2	98.90	98.94	99.51(8)	99.68	99.82(7)	100.10(7)	100.00(7)	100.06(6)	100.5(2)	100.22(7)	100.27(10)
O3—Ti2—O2	156.74	156.33	155.50(7)	155.43	155.13(6)	154.71(7)	154.53(8)	154.36(6)	154.1(2)	153.94(7)	153.64(10)
O10—Ti2—O2	76.90	76.85	77.11(7)	77.27	77.23(6)	77.36(6)	77.51(7)	77.67(5)	77.4(2)	77.79(6)	77.88(9)
O7—Ti2—O4	101.64	101.48	101.93(8)	102.39	102.36(6)	102.44(7)	102.73(7)	102.98(6)	103.1(2)	103.29(7)	103.40(10)
O8—Ti2—O4	156.76	156.06	155.40(7)	155.21	154.84(6)	154.59(6)	154.34(7)	154.11(5)	153.9(2)	153.63(7)	153.51(9)
O3—Ti2—O4	81.51	80.83	80.33(7)	80.08	79.83(6)	79.68(6)	79.45(7)	79.12(5)	79.0(2)	78.89(7)	78.88(9)
O10—Ti2—O4	72.21	71.91	71.60(6)	71.60	71.56(5)	71.47(6)	71.47(6)	71.50(5)	71.7(2)	71.33(6)	71.54(8)
O2—Ti2—O4	78.04	78.14	77.44(7)	77.48	77.34(6)	76.95(6)	76.87(7)	77.01(5)	77.0(2)	76.75(6)	76.34(9)
CShM (Oct)	**1.241**	**1.305**	**1.397**	**1.426**	**1.472**	**1.512**	**1.545**	**1.573**	**1.619**	**1.634**	**1.662**

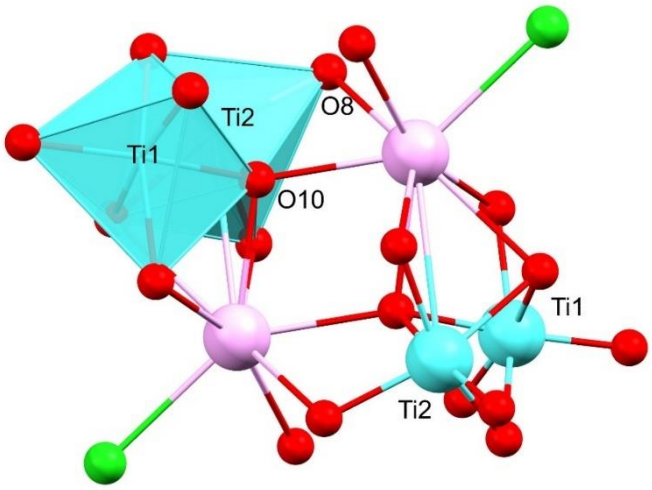

Figure S4 Detailed polyhedral representation of the metal-oxo core of the **Ti_4Ln_2** cage. The Ti2 octahedron is the one sharing its edge with Ln^{3+} (the "bridging" octahedron), whereas the Ti1 octahedron sits more to the periphery of the complex. The distortion of the Ti2 octahedron is reflected in the O8-Ti2-O10 angle, which shows a steady decrease across the series of lanthanides, as Ln^{3+} gets smaller (see Table S4).

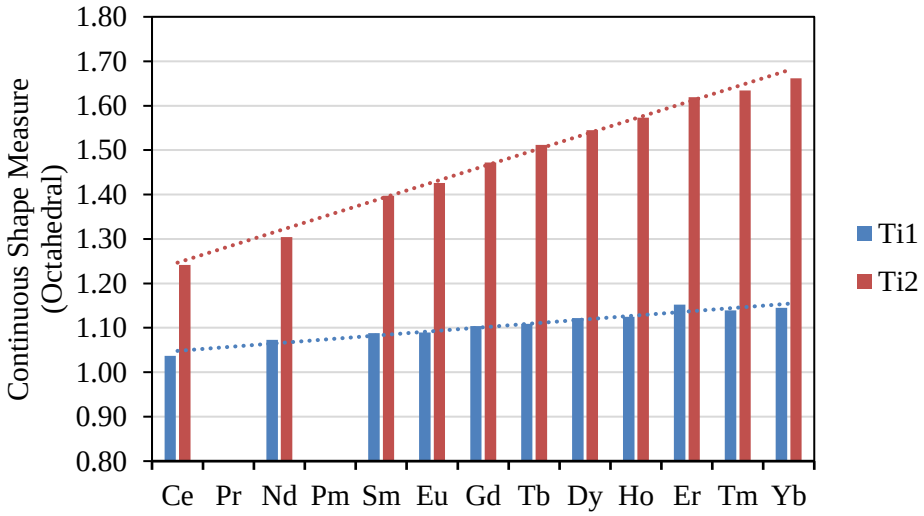

Figure S5 Graphical representation of the CShM obtained for the series of **Ti_4Ln_2** cages for the Ti1 and Ti2 octahedron (Figure S3). The Ti2 octahedron is found to be significantly more distorted than the Ti1 octahedron. The steeper gradient across the series for the Ti2 octahedron indicates a larger influence of Ln^{3+} on the distortion compared to the Ti1 octahedron. No crystallographic data are available for Ln = Pr and Pm.

Table S4 Ln-Cl and Ln-O bond lengths for the novel **Ti_4Ln_2** cages (Ln = Sm, Gd, Tb, Dy, Ho, Er, Tm, Yb) [Å].

	Ti_4Sm_2	**Ti_4Gd_2**	**Ti_4Tb_2**	**Ti_4Dy_2**	**Ti_4Ho_2**	**Ti_4Er_2**	**Ti_4Tm_2**	**Ti_4Yb_2**
Ln—Cl1	2.6927(6)	2.6721(5)	2.6529(5)	2.6423(6)	2.6324(5)	2.6225(18)	2.6120(6)	2.6011(8)
Ln—O1	2.4599(17)	2.4436(14)	2.4299(15)	2.4226(16)	2.4109(13)	2.403(5)	2.3951(16)	2.384(2)
Ln—O3	2.4614(16)	2.4391(14)	2.4265(15)	2.4162(17)	2.4037(12)	2.386(5)	2.3859(16)	2.382(2)
Ln—O4	2.5778(17)	2.5559(14)	2.5448(15)	2.5378(17)	2.5279(12)	2.518(5)	2.5114(16)	2.515(2)
Ln—O8[a]	2.4772(17)	2.4501(15)	2.4377(15)	2.4256(18)	2.4109(13)	2.386(6)	2.3894(16)	2.380(2)
Ln—O9	2.4464(18)	2.4226(15)	2.4056(15)	2.3939(16)	2.3822(13)	2.360(5)	2.3581(16)	2.340(2)
Ln—O10	2.3887(15)	2.3656(13)	2.3489(13)	2.3348(15)	2.3233(12)	2.312(5)	2.2976(14)	2.2871(19)
Ln—O10[a]	2.3758(16)	2.3598(13)	2.3401(14)	2.3302(15)	2.3187(12)	2.316(5)	2.3002(15)	2.287(2)
(Ln—O)ave	**2.455**	**2.434**	**2.419**	**2.409**	**2.397**	**2.383**	**2.377**	**2.368**

Symmetry code: a = 1–x, 1–y, 1–z

Table S5 Ln-Cl and Ln-O bond lengths for previously published **Ti_4Ln_2** cages (Ln = Ce, Nd, Eu) [Å].

	Ti_4Ce_2 ZIWYEM	**Ti_4Nd_2 DEJRIV**	**Ti_4Eu_2 CURJEG**
Ln—Cl1	2.756	2.723	2.684
Ln—O1	2.522	2.485	2.456
Ln—O3	2.523	2.488	2.454
Ln—O4	2.653	2.605	2.575
Ln—O8	2.529	2.501	2.466
Ln—O9	2.521	2.481	2.439
Ln—O10	2.459	2.405	2.369
Ln—O10	2.438	2.422	2.378
(Ln—O)ave	**2.521**	**2.484**	**2.461**

Table S6 Ln-Cl and Ln-O bond lengths for previously published **Ti_8Ln** cages (Ln = Ce, Er) [Å].

	Ti_8Ce ZIWYAI	**Ti_8Er ORIFAY**
Ln—O	2.418	2.305
Ln—O	2.420	2.345
Ln—O	2.518	2.364
Ln—O	2.563	2.339
Ln—O	2.418	2.312
Ln—O	2.420	2.352
Ln—O	2.518	2.356
Ln—O	2.563	2.345
Ln—O(ethanol)	2.069	—
(Ln—O)ave	**2.436**	**2.340**

Table S7 Continuous Shape Measure (CShM) for Ti_8Ln cages.

Ti_8Ce (ZIWYAI)		**Ti_8Er (ORIFAY)**		
Ti1	1.200	Ti1	1.219	[Part of face-sharing pair]
Ti2	1.108	Ti2	1.185	[Part of face-sharing pair]
Ti2A	1.108	Ti3	1.152	[Part of face-sharing pair]
Ti1A	1.200	Ti4	1.201	[Part of face-sharing pair]
Ti3A	0.843	Ti5	0.817	[Part of edge-sharing TiO core]
Ti3	0.843	Ti6	0.830	[Part of edge-sharing TiO core]
Ti4	1.694	Ti7	1.635	[Part of edge-sharing TiO core]
Ti4A	1.694	Ti8	1.630	[Part of edge-sharing TiO core]

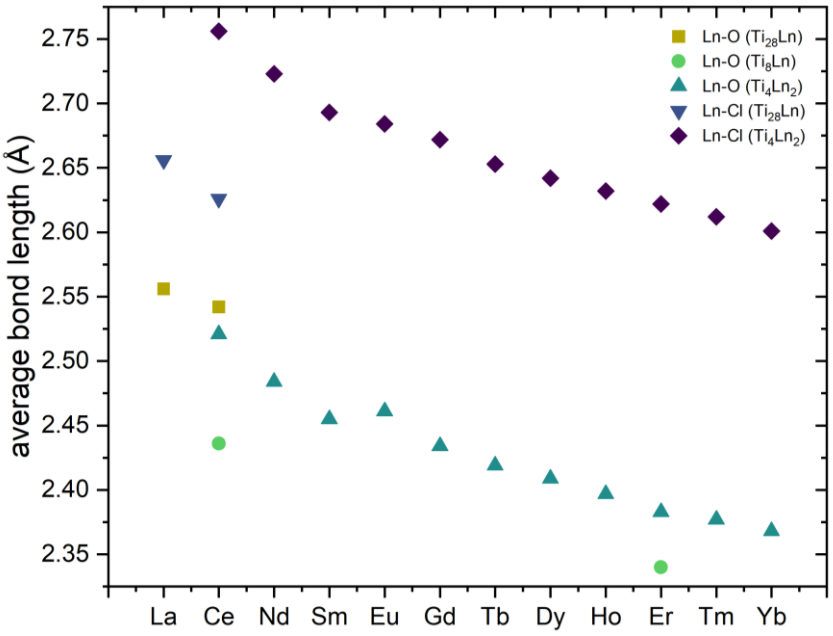

Figure S6 Comparison of the average Ln-O and Ln-Cl bond lengths in **$Ti_{28}Ln$**, **Ti_8Ln** and **Ti_4Ln_2** cages based on the structural data in Tables S4-S6. A decreasing trend is observed along the series of lanthanides, which is in agreement with the decreasing ionic radius of Ln^{3+} and the resulting increase in Lewis acidity.

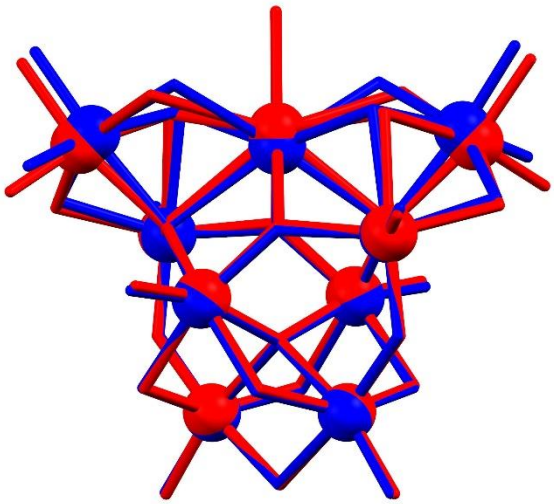

Figure S7 Structural overlay of the two **Ti_8Ln** cages (Ln = Ce [red] and Er [blue]). The geometry of the lower section of the complexes (comprising edge-sharing octahedra) is essentially identical. The upper TiO_6 octahedra show some flexibility in the Ln^{3+} binding site: For **Ti_8Ce** the octahedra are tilted away from Ce^{3+}, and the additional EtOH molecule is coordinated above the binding site. For **Ti_8Er** the octahedra are tilted further towards Er^{3+} and there is no additional coordination.

Magnetic measurements

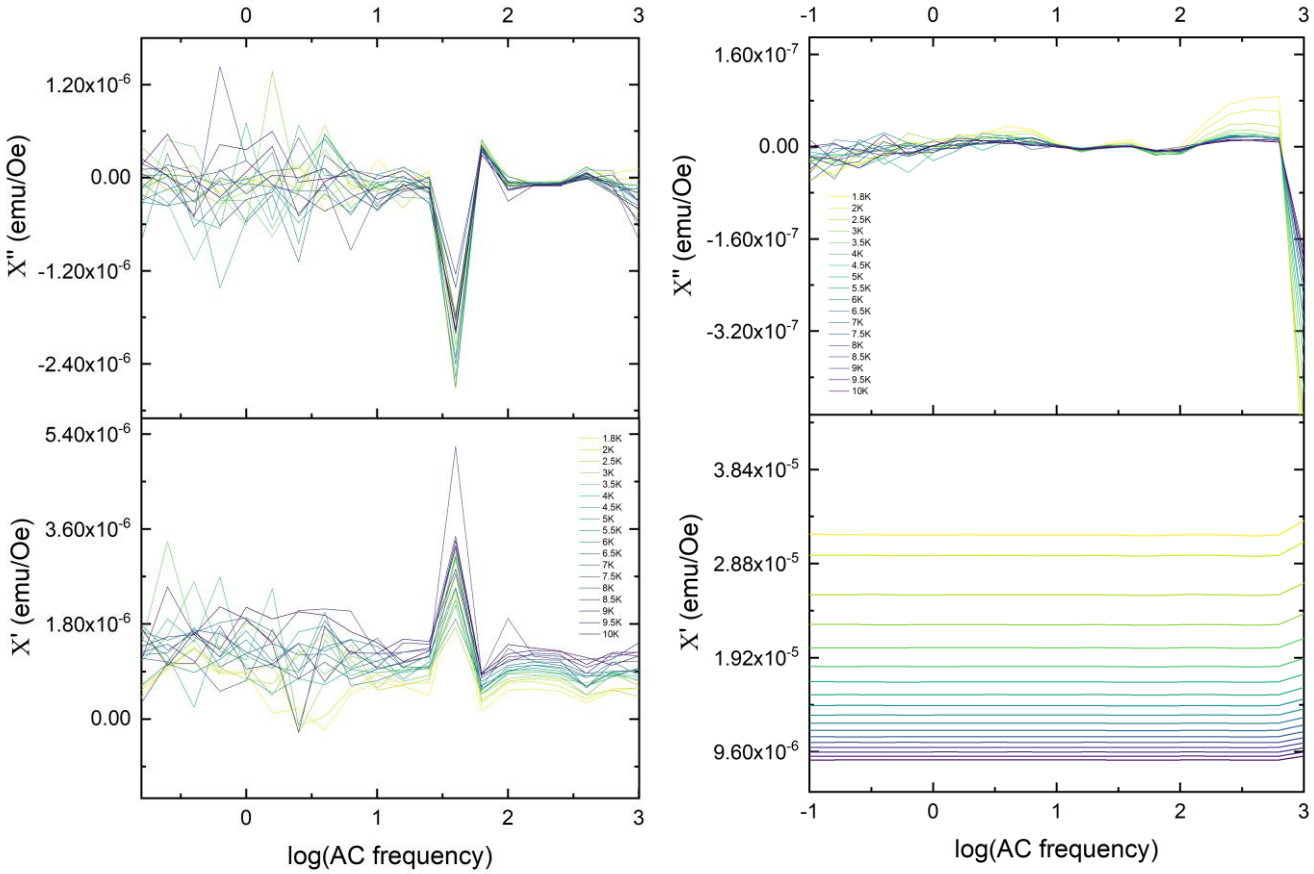

Figure S8 AC susceptibility measurements at various temperatures between 0.1 and 1000 Hz of Dy_2Ti_4 (left) and Ho_2Ti_4 (right). Some temperature independent features are observed in the Dy sample at around 60 Hz, which might result from sample movement during the measurement and can't be assigned to a relaxation response. No features are seen in case of Ho.

Decomposition studies

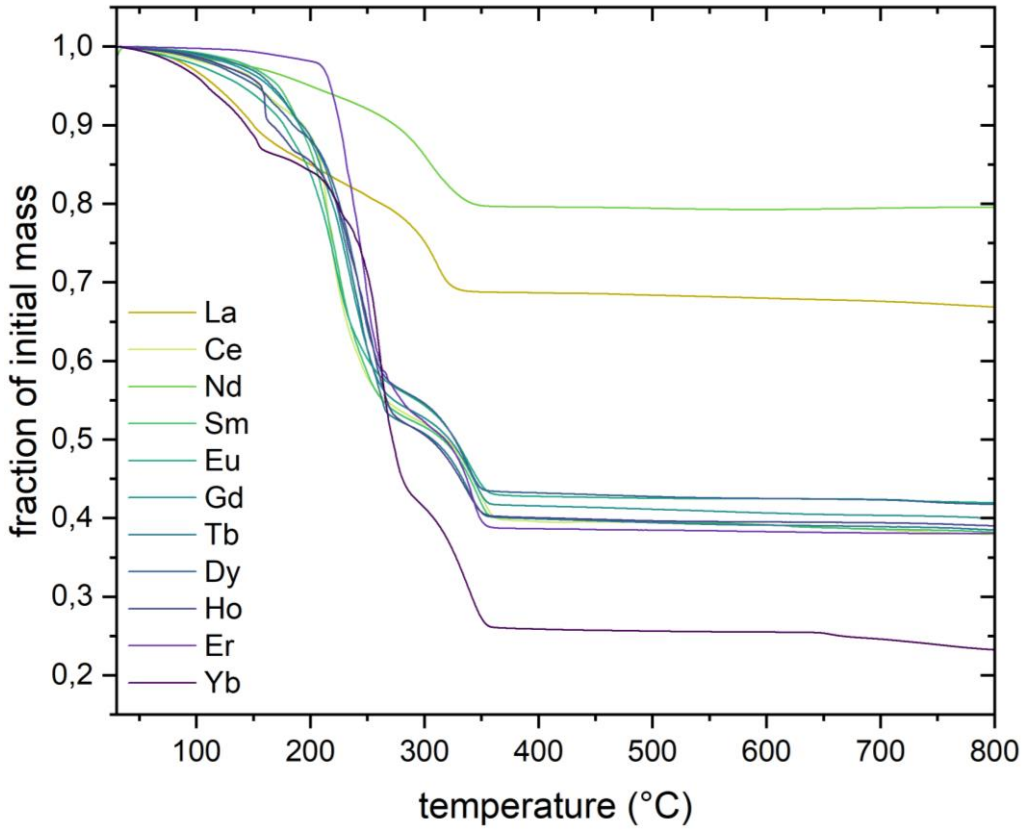

Figure S9 TGA curves for all Ln-POTs synthesised in this work. The measurements were carried out under nitrogen between 30-800°C. Distinct curves are observed for lanthanum (**$Ti_{28}La$**), neodymium (**Ti_4Nd_2**) and erbium (**Ti_8Er**). The remaining lanthanides (**Ti_4Ln_2**) show similar thermal decomposition steps.

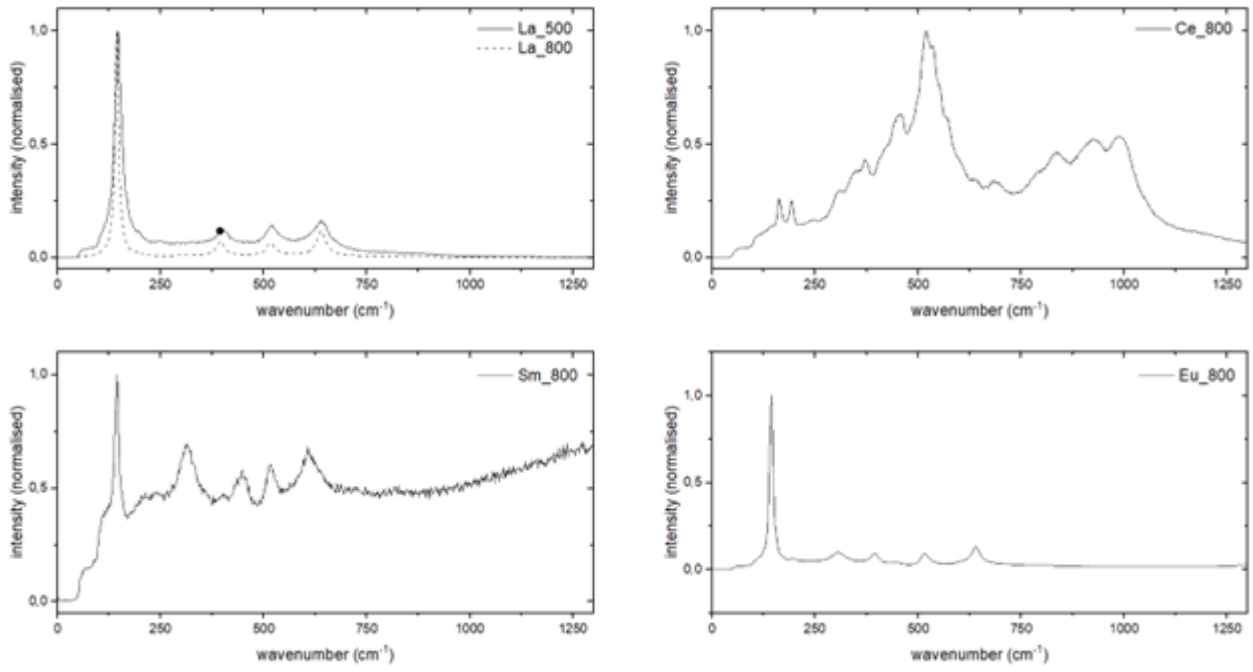

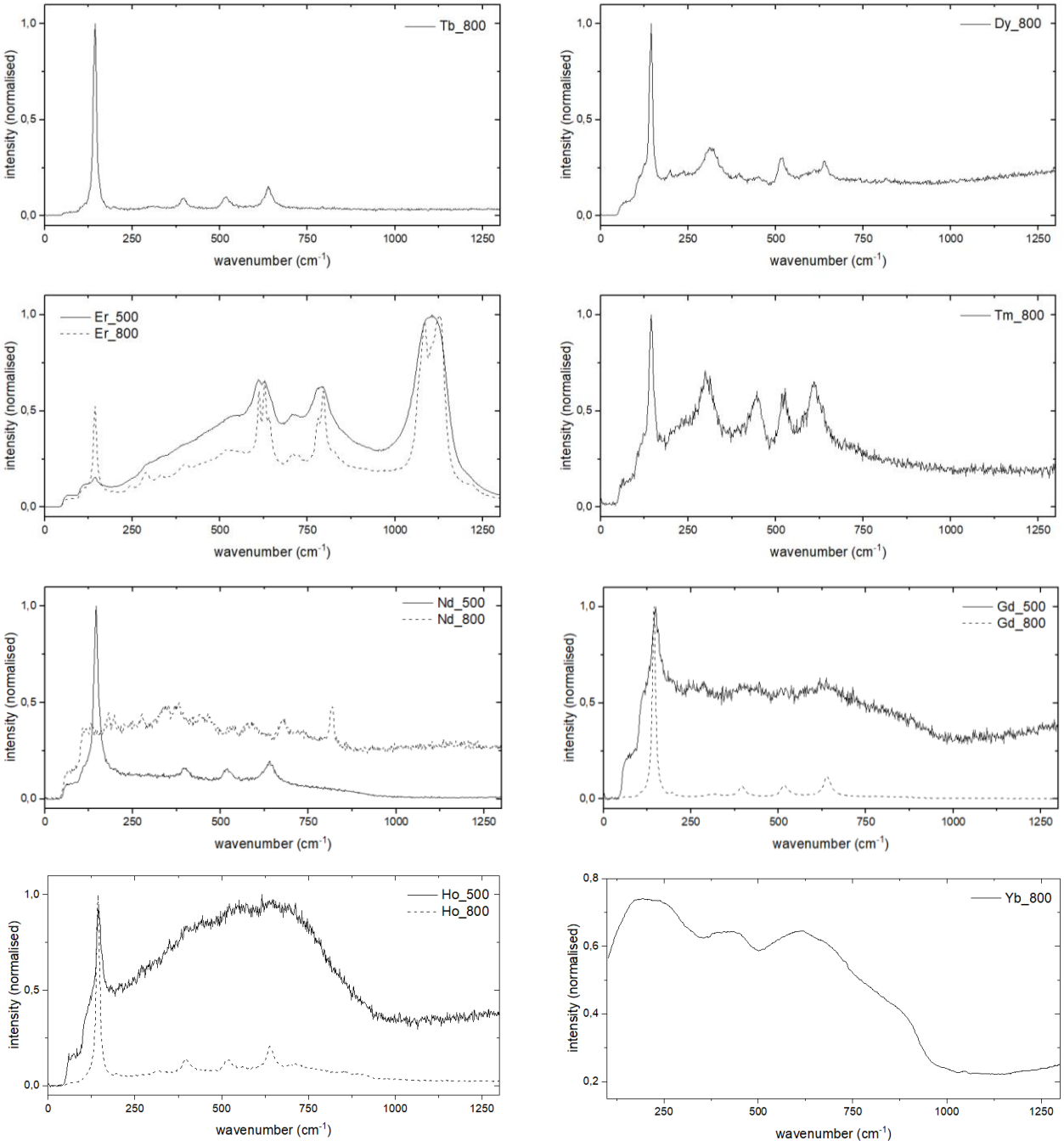

Figure S10 Raman spectra of all Ln-TiO_2 samples obtained from hydrolytic decomposition and annealing at 500 and 800°C. The spectra of 500°C-samples show poor crystallinity and were excluded where no significant peaks were visible. However, for Ln = La, Nd, Gd, Ho and Er the formation of the main component anatase (144, 197, 399, 516, 639 cm^{-1}) can be observed even at lower temperatures. Additional peaks account for the formation of $Ln_4Ti_9O_{24}$ (Ln = Nd) or $Ln_2Ti_2O_7$.

SEM measurements

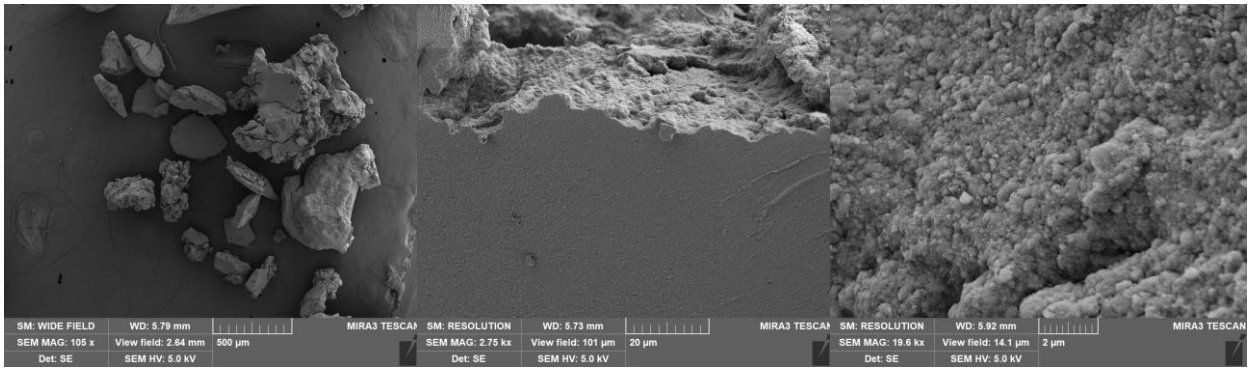

Figure S11 Crystalline particles of Sm-TiO_2 after annealing to 800°C under air. Viewing fields are chosen to be 2.5 mm, 100 µm and 15 µm (left to right).

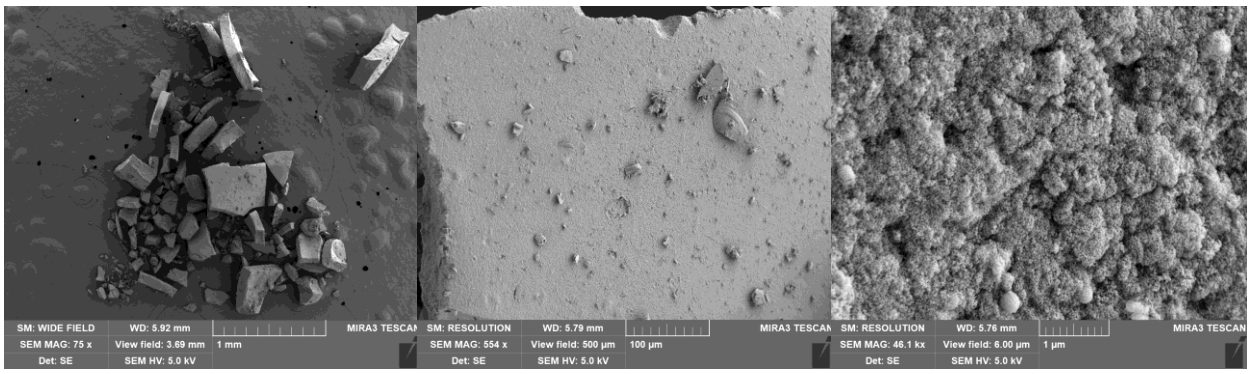

Figure S12 Crystalline particles of Gd-TiO_2 after annealing to 800°C under air. Viewing fields are chosen to be 3.7 mm, 500 µm and 6 µm (left to right).

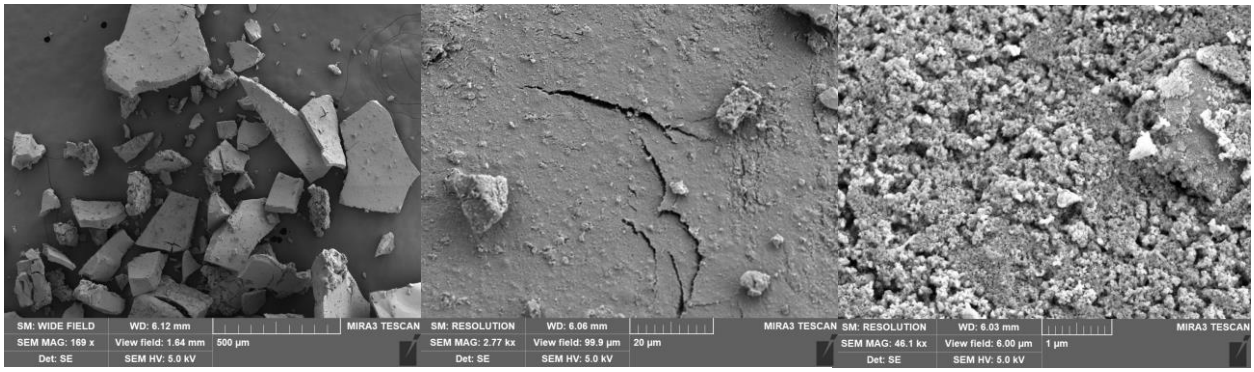

Figure S13 Crystalline particles of Tb-TiO_2 after annealing to 800°C under air. Viewing fields are chosen to be 1.6 mm, 100 µm and 6 µm (left to right).

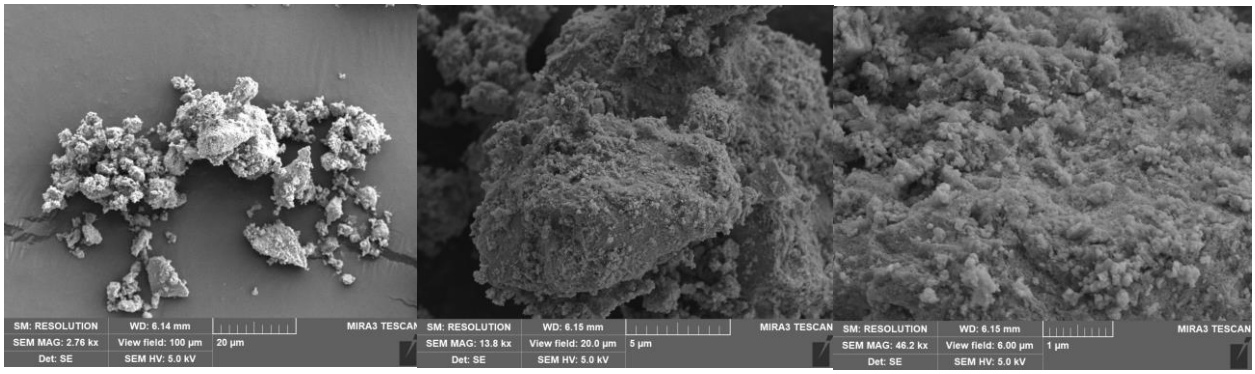

Figure S14 Crystalline particles of Dy-TiO_2 after annealing to 800°C under air. Viewing fields are chosen to be 100 µm, 60 µm and 6 µm (left to right).

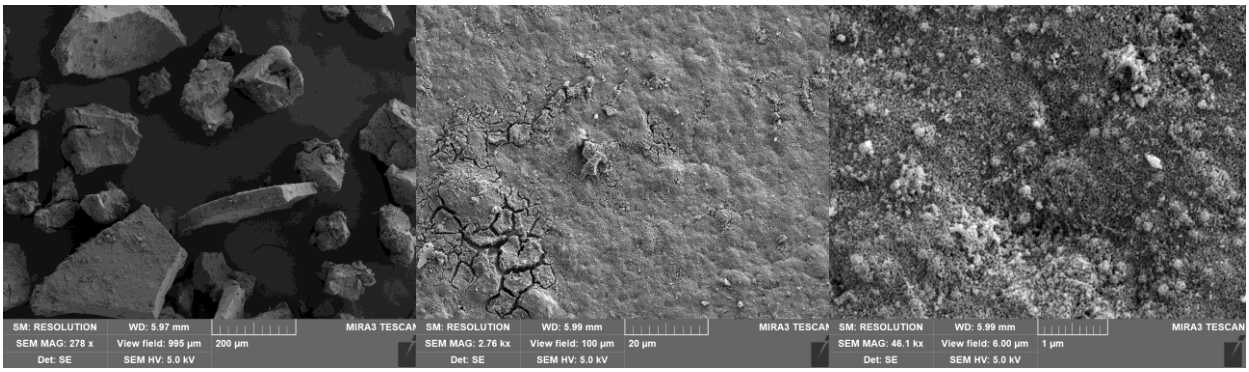

Figure S15 Crystalline particles of Ho-TiO_2 after annealing to 800°C under air. Viewing fields are chosen to be 200 µm, 20 µm and 6 µm (left to right).

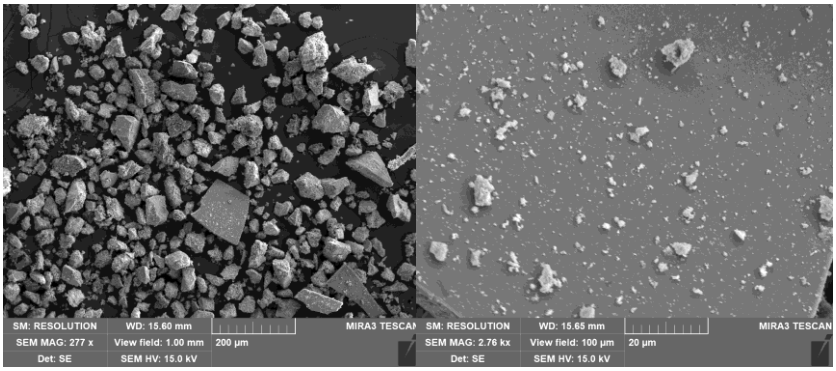

Figure S16 Crystalline particles of Tm-TiO_2 after annealing to 800°C under air. Viewing fields are chosen to be 200 µm and 20 µm (left to right).

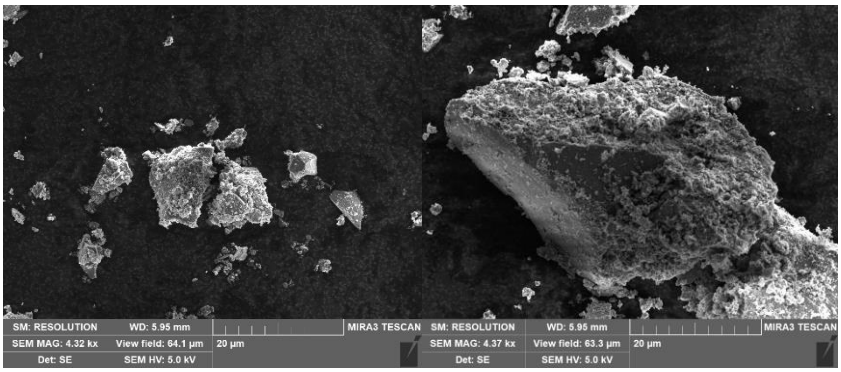

Figure S17 Crystalline particles of Yb-TiO_2 after annealing to 800°C under air. Viewing fields are chosen to be 60 µm.

EDX measurements

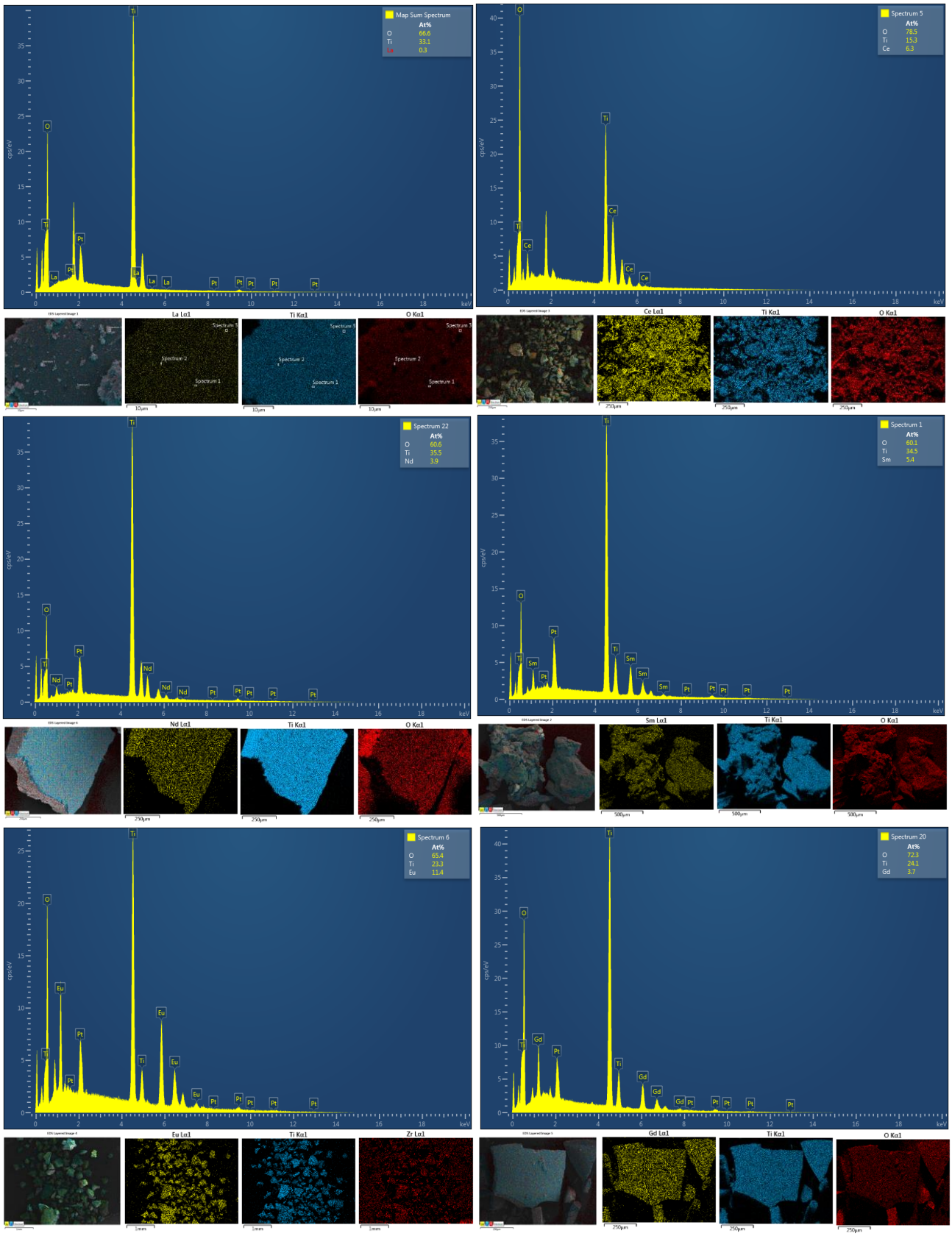

Figure S18 Map EDX spectra (at%) and elemental distribution of the decomposed Ln-TiO_2 samples for Ln = La, Ce, Nd, Sm, Eu and Gd (ltr, ttb). The samples were sputtered with Pt prior to measurements, which explains the Pt peaks (unassigned) in the spectra.

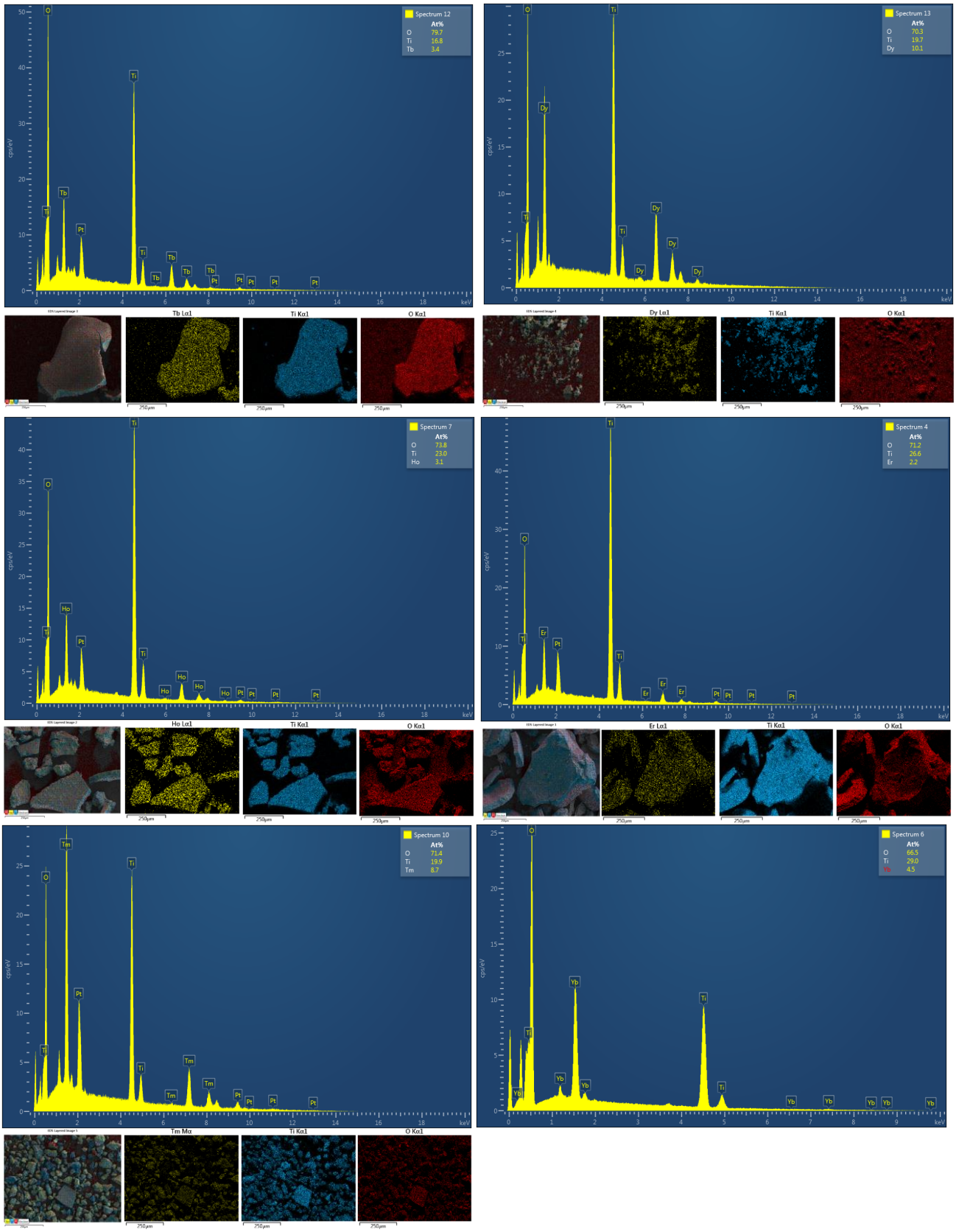

Figure S19 Map EDX spectra (at%) and elemental distribution of the decomposed Ln-TiO_2 samples for Ln = Tb, Dy, Ho, Er, Tm and Yb (ltr, ttb). The samples were sputtered with Pt prior to measurements, which explains the Pt peaks (unassigned) in the spectra.

Rietveld refinements

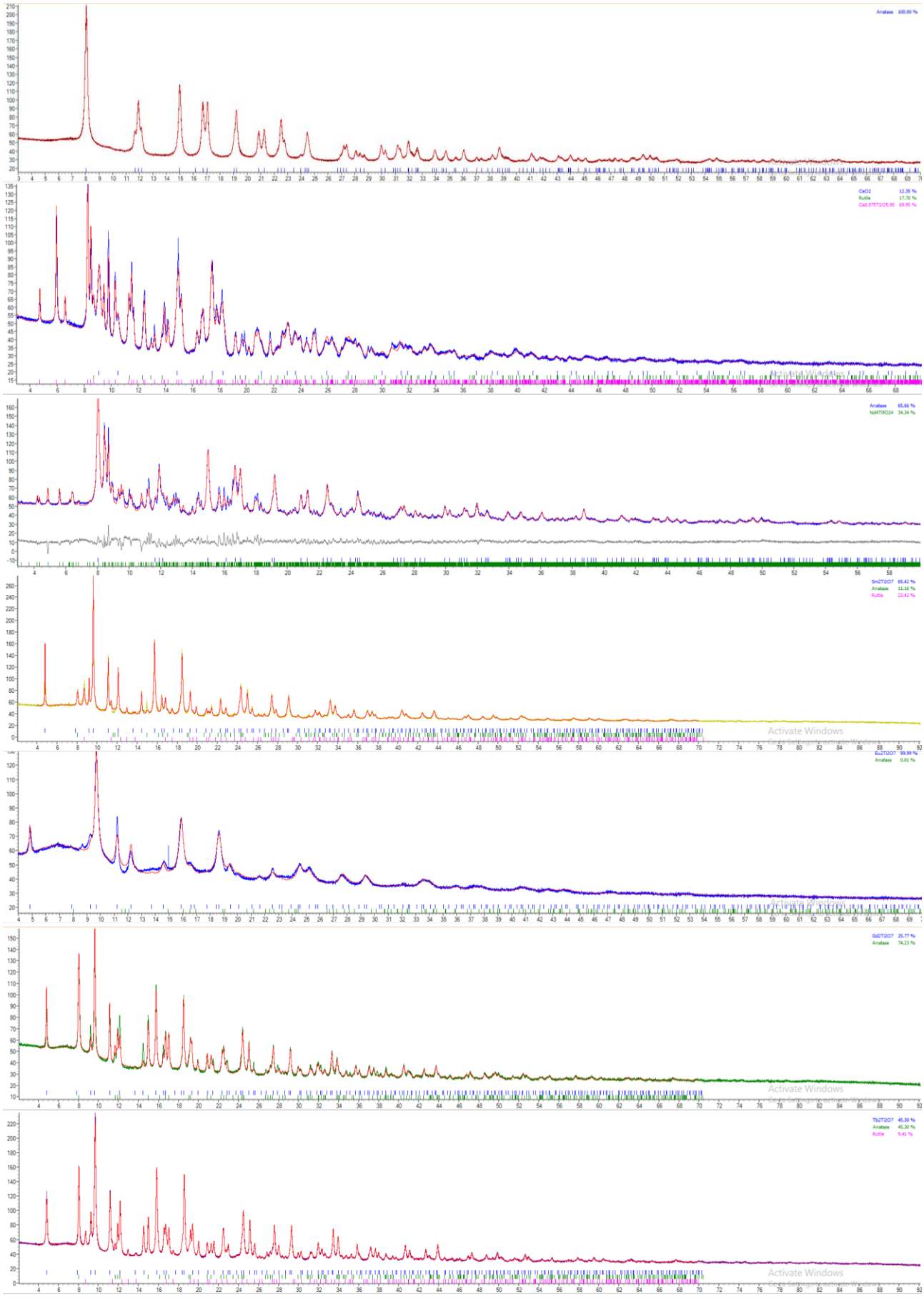

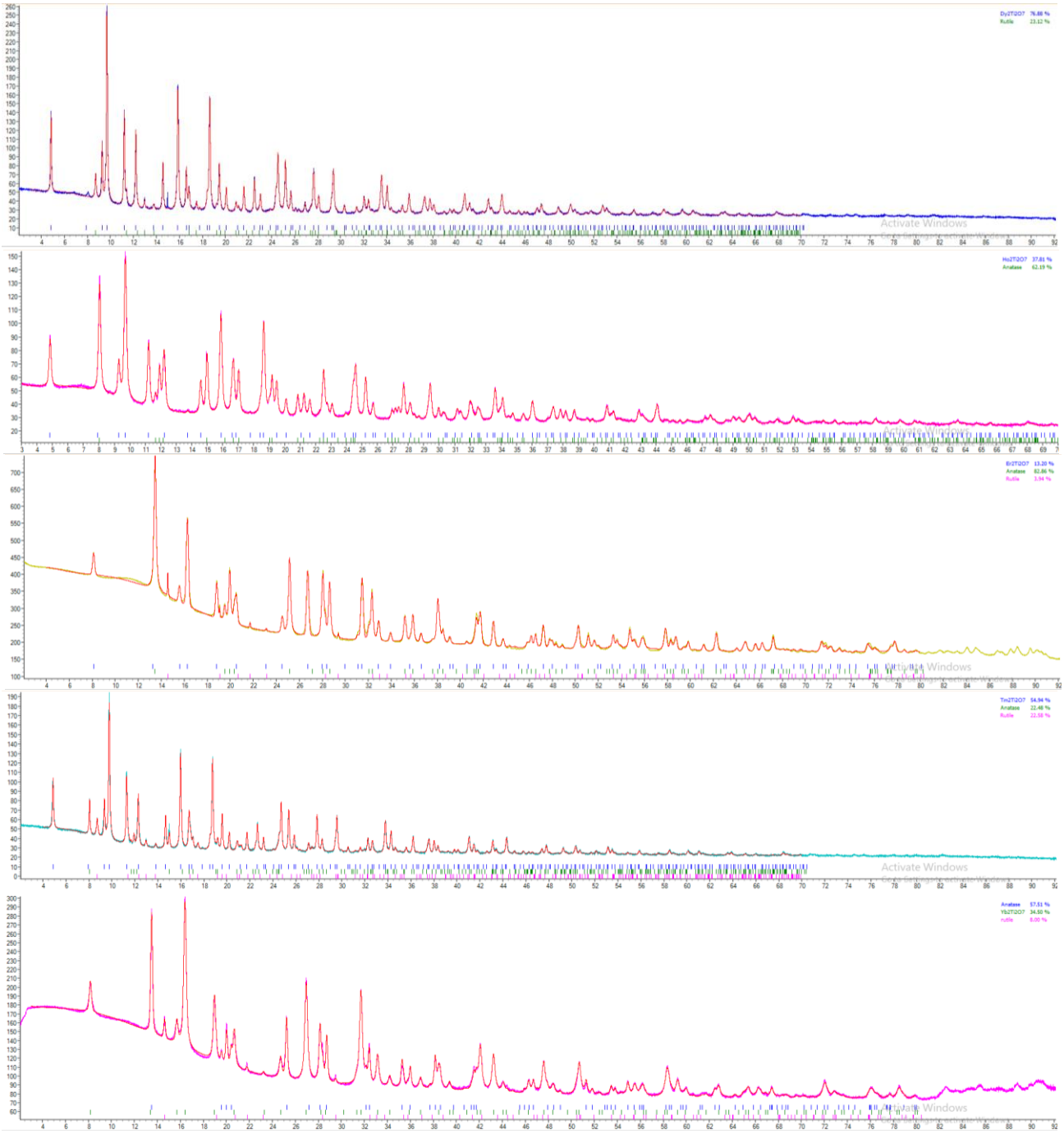

Figure S20 Measured powder patterns and the fitted curves (red) obtained from Rietveld refinements on Topas Academic for Ln/TiO hybrid materials (from top to bottom; Ln = La, Ce, Nd, Sm, Eu, Gd, Tb, Dy, Ho, Er, Tm, Yb). The peak positions of the single phases are indicated as tick marks below. The data was refined against a silicon standard at 0.82443 Å (Ln=Er) or 0.49381 Å.

Ln	site mixing	R_{wp}	R_{exp}	GoF
La	-	4.53	2.56	1.77
Ce	-	9.68	2.68	3.61
Nd	-	7.49	2.19	4.42
Sm	$Sm_{1.7}Ti_{2.3}O_7$	8.41	2.33	3.60
Eu	$Eu_{1.5}Ti_{2.5}O_7$	6.13	2.47	2.48
Gd	$Gd_{2.3}Ti_{0.7}O_7$	8.83	2.71	3.25
Tb	$Tb_{2.03}Ti_{1.97}O_7$	5.65	2.25	2.51
Dy	$Dy_{1.95}Ti_{2.05}O_7$	5.28	2.65	1.99
Ho	$Ho_{1.83}Ti_{2.13}O_7$	4.01	2.65	1.51
Er	-	2.96	0.39	7.56
Tm	$Tm_{2.07}Ti_{1.93}O_7$	6.19	2.92	2.12
Yb	$Yb_{2.18}Ti_{0.82}O_7$	2.67	0.89	3.01

Table S8 Selected refinement parameters for Ln-TiO_2.

UV-Vis measurements

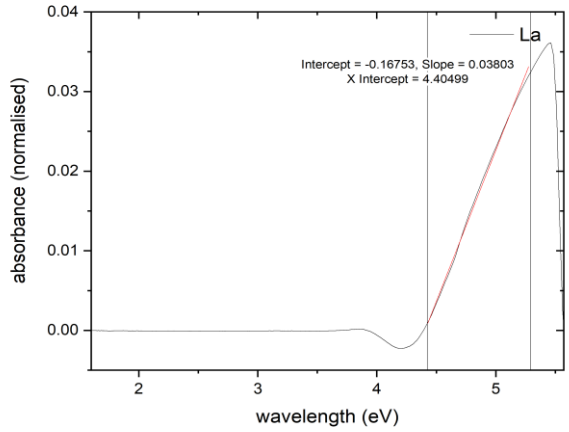

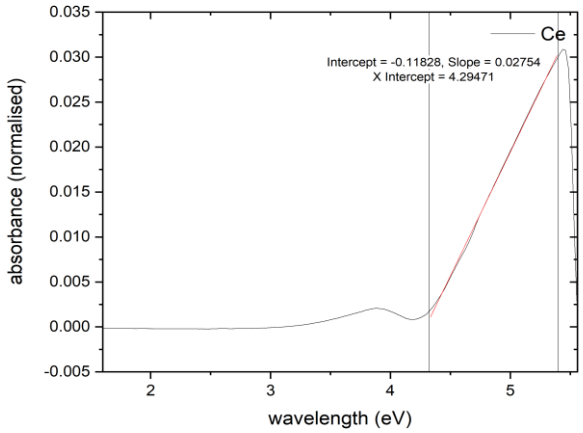

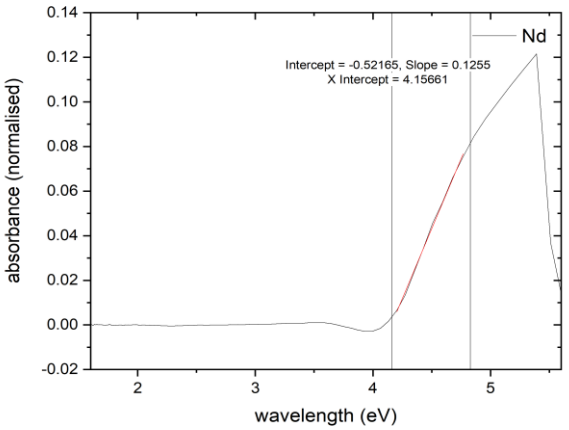

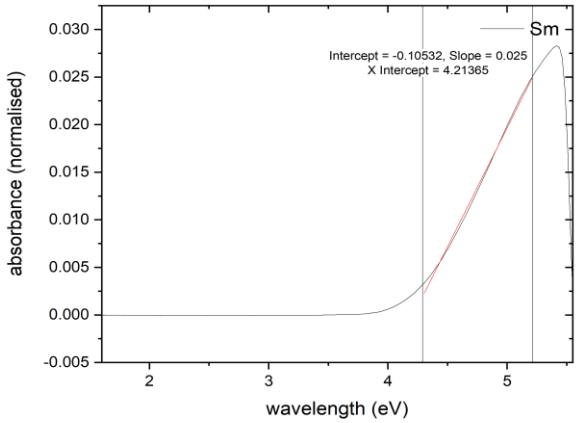

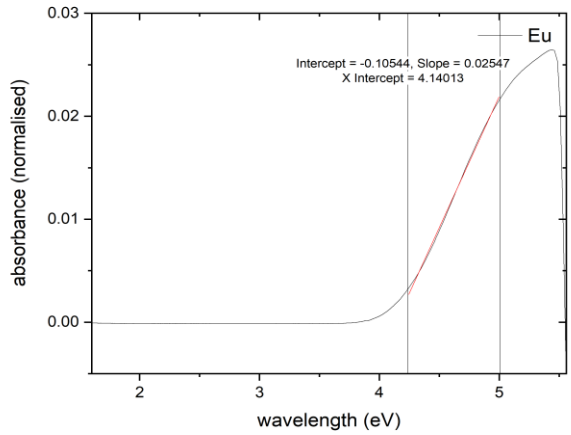

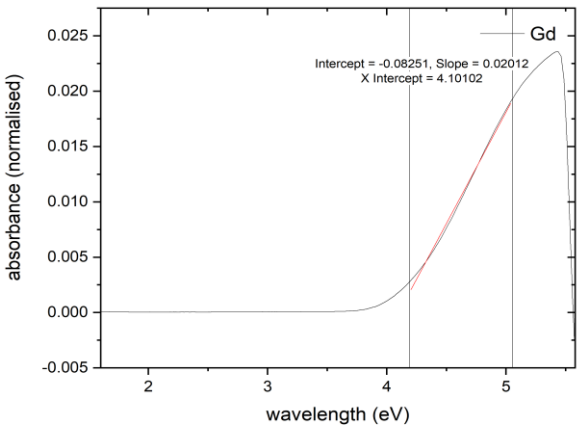

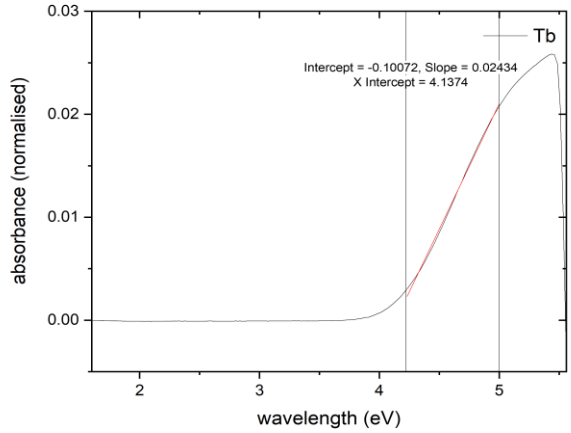

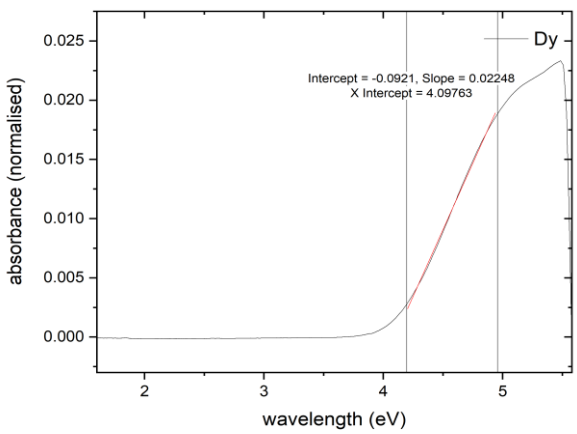

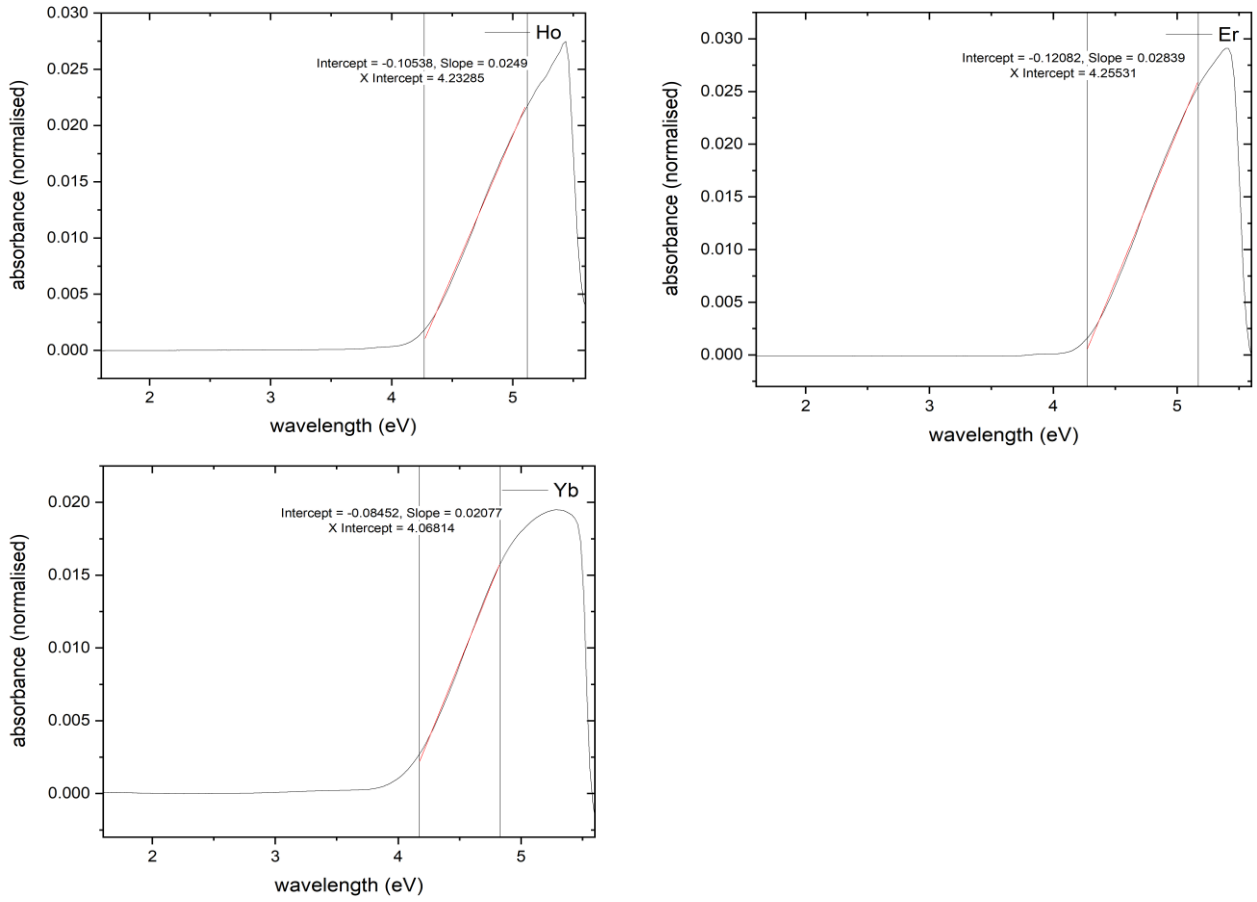

Figure S21 Solution-state UV-Vis spectra of the Ln-POT compounds (0.033 mg/mL in DCM) and the linear extrapolation of the main absorption peak (O(p) → Ti(d) in the Ti_xO_y-framework). The X intercept is taken as an estimate of the HOMO-LUMO gap of the compounds. Errors are estimated to be around ± 0.1 eV.

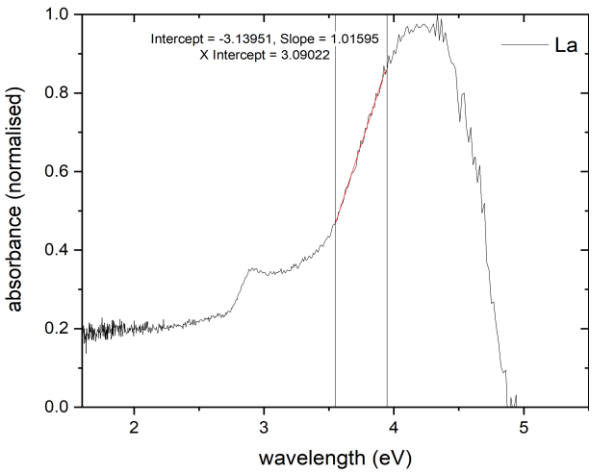
Intercept = -3.13951, Slope = 1.01595
X Intercept = 3.09022
La
absorbance (normalised)
wavelength (eV)

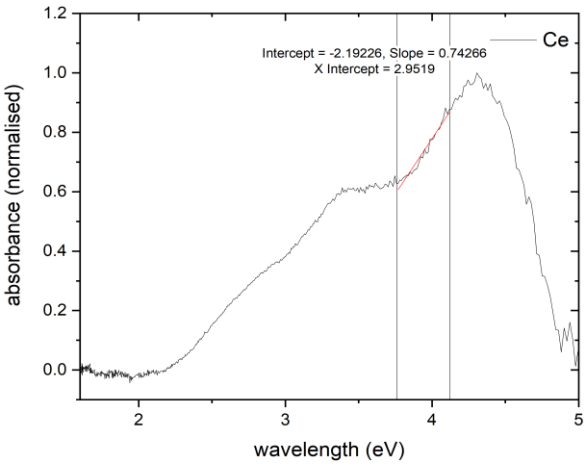
Intercept = -2.19226, Slope = 0.74266
X Intercept = 2.9519
Ce
absorbance (normalised)
wavelength (eV)

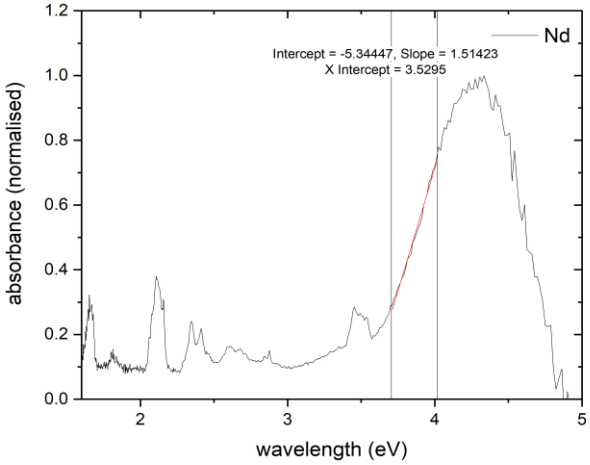
Intercept = -5.34447, Slope = 1.51423
X Intercept = 3.5295
Nd
absorbance (normalised)
wavelength (eV)

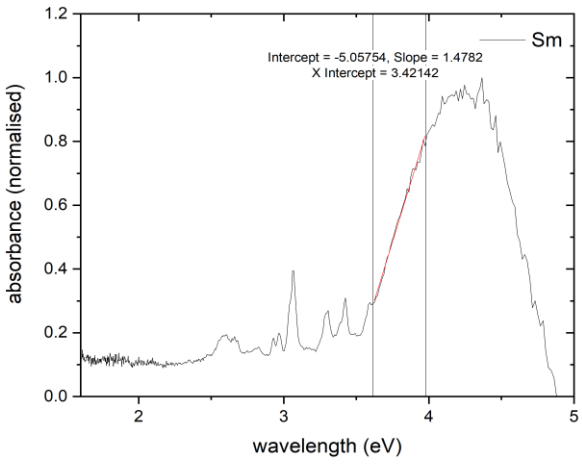
Intercept = -5.05754, Slope = 1.4782
X Intercept = 3.42142
Sm
absorbance (normalised)
wavelength (eV)

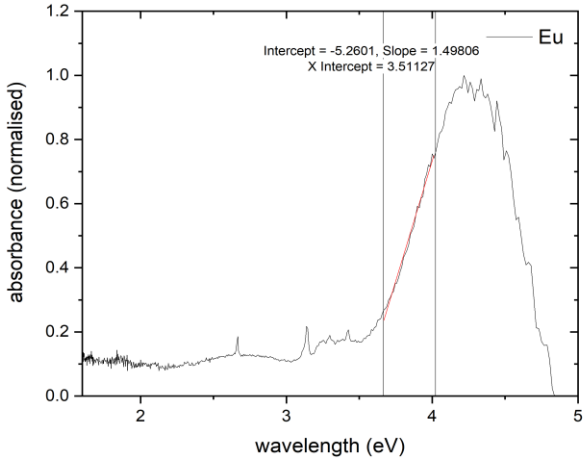
Intercept = -5.2601, Slope = 1.49806
X Intercept = 3.51127
Eu
absorbance (normalised)
wavelength (eV)

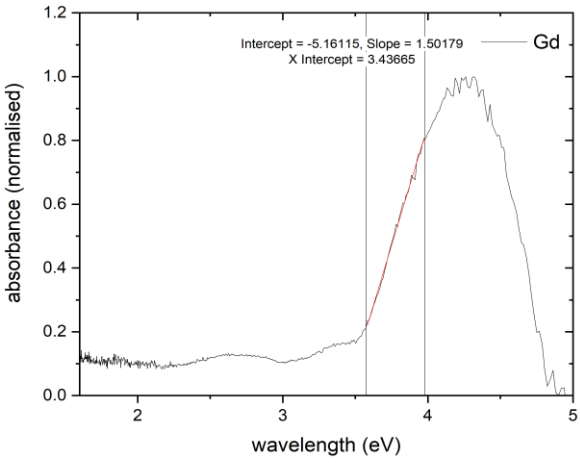
Intercept = -5.16115, Slope = 1.50179
X Intercept = 3.43665
Gd
absorbance (normalised)
wavelength (eV)

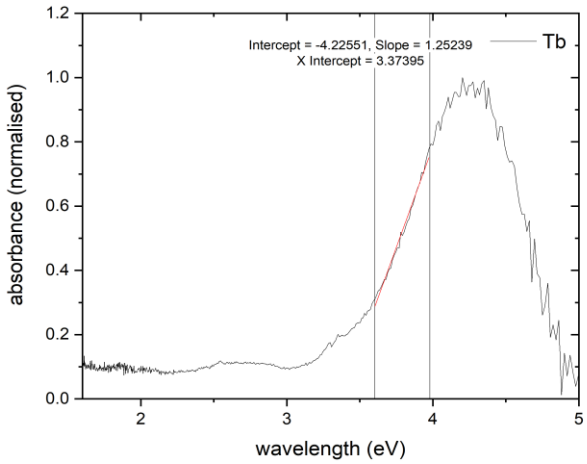
Intercept = -4.22551, Slope = 1.25239
X Intercept = 3.37395
Tb
absorbance (normalised)
wavelength (eV)

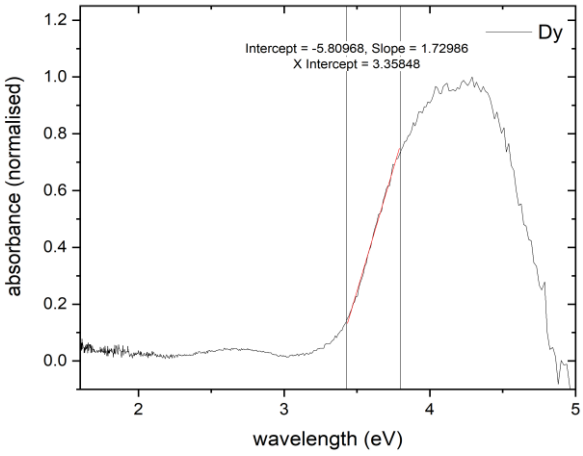
Intercept = -5.80968, Slope = 1.72986
X Intercept = 3.35848
Dy
absorbance (normalised)
wavelength (eV)

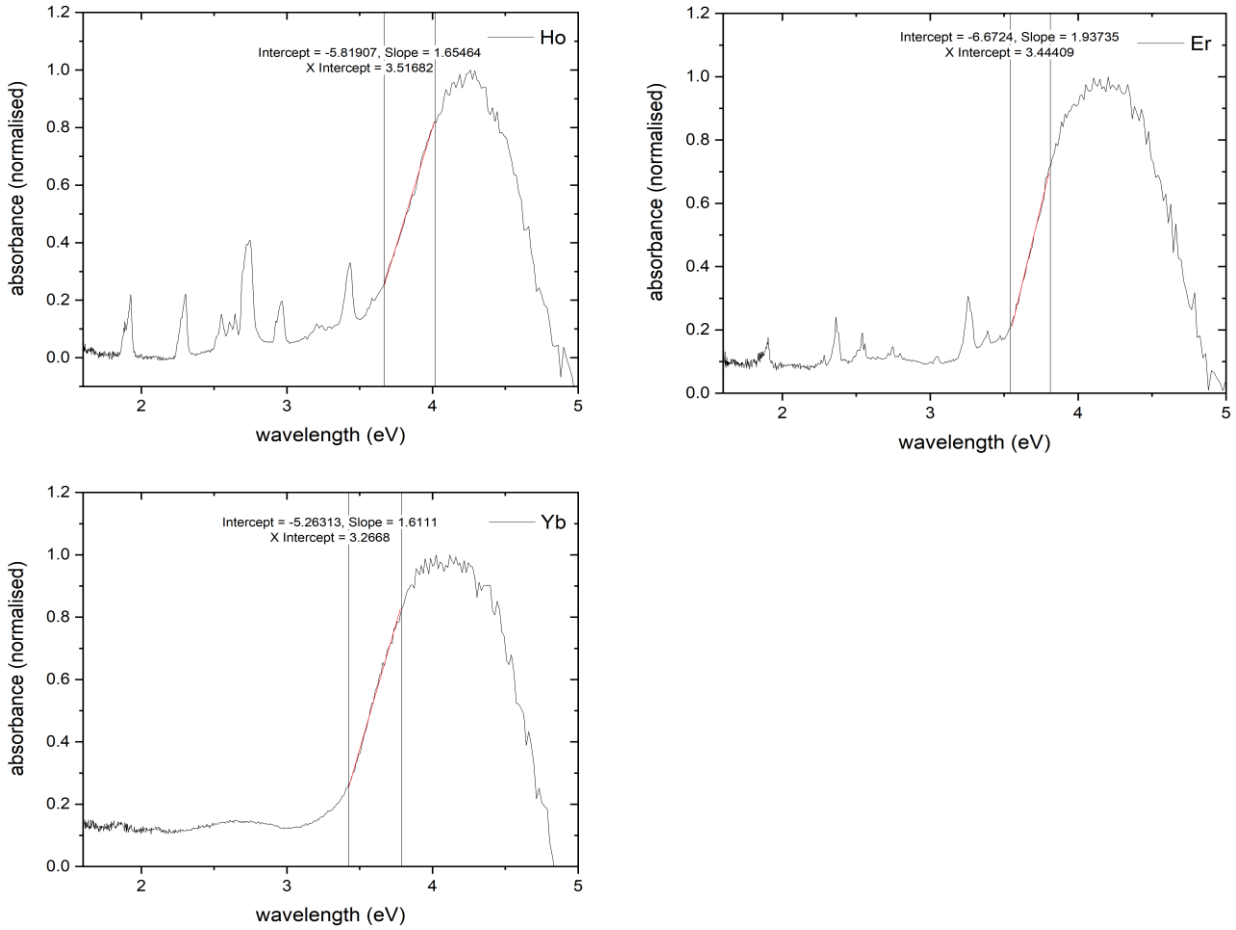

Figure S22 Solid-state UV-Vis spectra of the Ln-POT compounds and the linear extrapolation of the main absorption peak (O(p) → Ti(d) in the Ti_xO_y-framework). The X intercept is taken as an estimate of the HOMO-LUMO gap of the compounds. Errors are estimated to be around ± 0.1 eV.

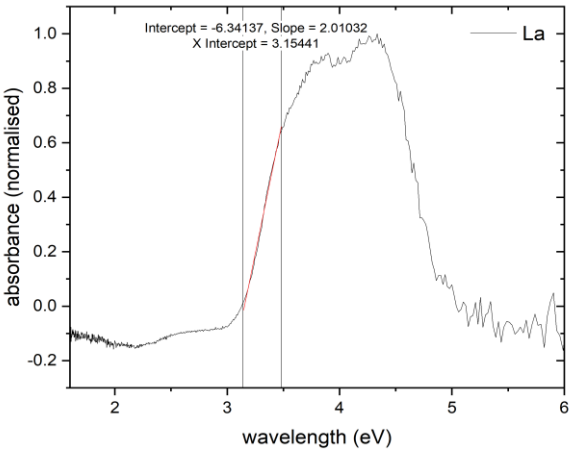
Intercept = -6.34137, Slope = 2.01032
X Intercept = 3.15441
La
absorbance (normalised)
wavelength (eV)

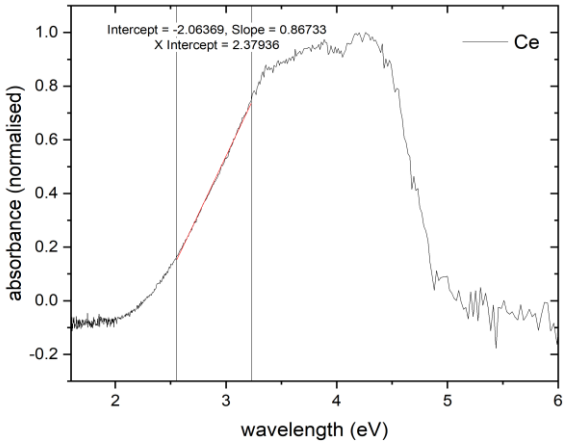
Intercept = -2.06369, Slope = 0.86733
X Intercept = 2.37936
Ce
absorbance (normalised)
wavelength (eV)

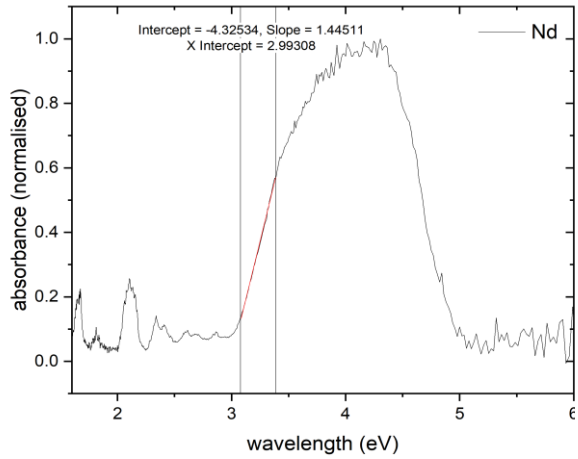
Intercept = -4.32534, Slope = 1.44511
X Intercept = 2.99308
Nd
absorbance (normalised)
wavelength (eV)

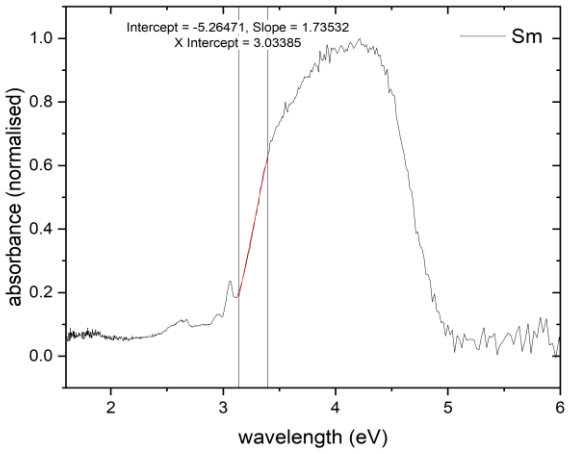
Intercept = -5.26471, Slope = 1.73532
X Intercept = 3.03385
Sm
absorbance (normalised)
wavelength (eV)

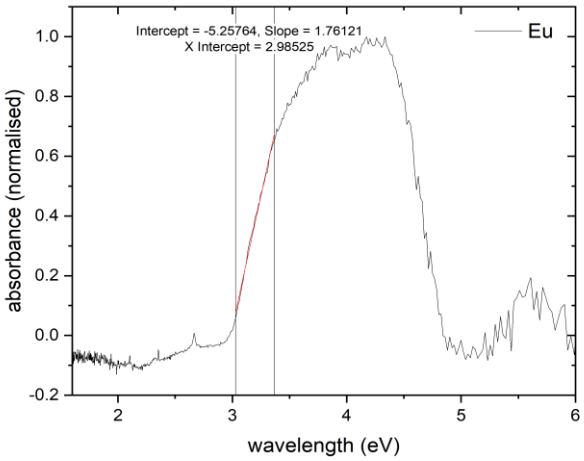
Intercept = -5.25764, Slope = 1.76121
X Intercept = 2.98525
Eu
absorbance (normalised)
wavelength (eV)

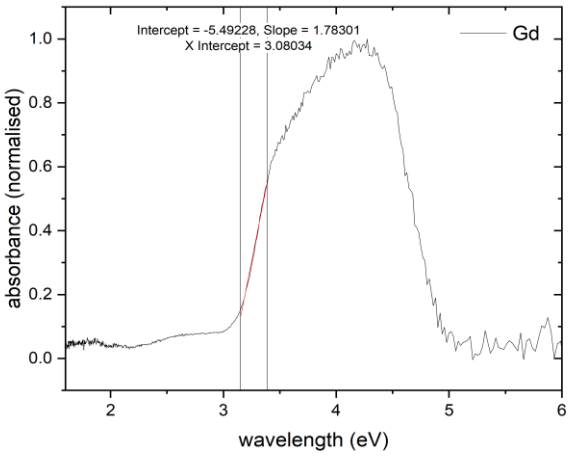
Intercept = -5.49228, Slope = 1.78301
X Intercept = 3.08034
Gd
absorbance (normalised)
wavelength (eV)

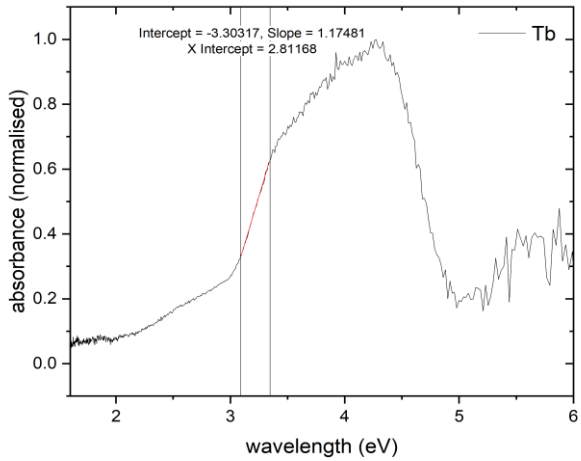
Intercept = -3.30317, Slope = 1.17481
X Intercept = 2.81168
Tb
absorbance (normalised)
wavelength (eV)

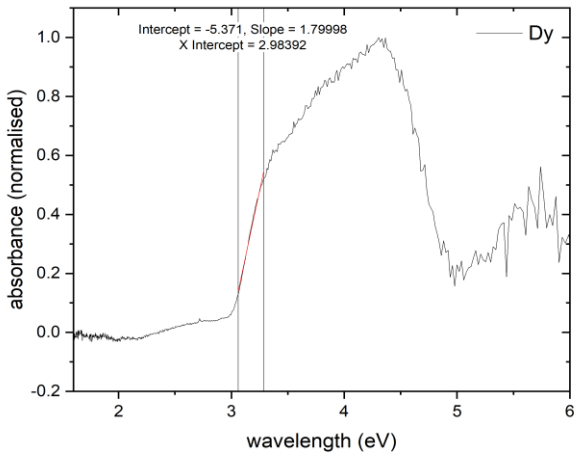
Intercept = -5.371, Slope = 1.79998
X Intercept = 2.98392
Dy
absorbance (normalised)
wavelength (eV)

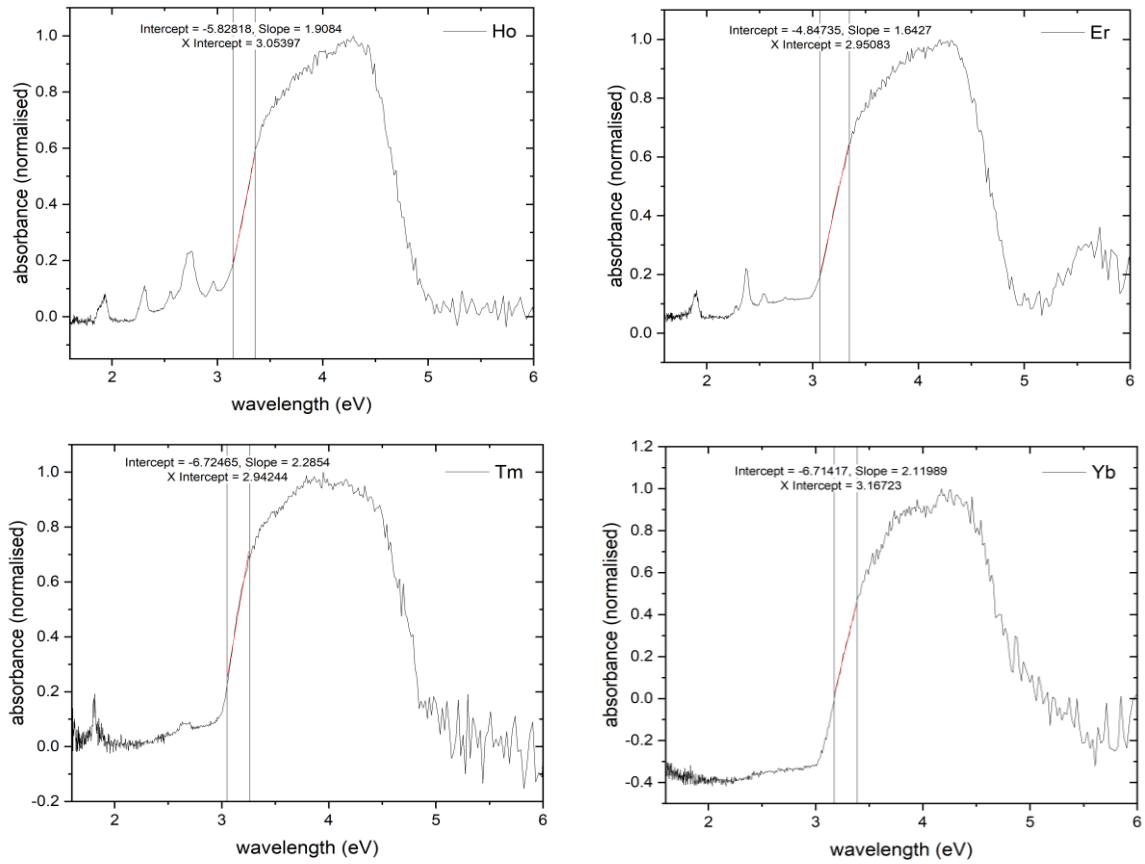

Figure S23 Solid-state UV-Vis spectra of the decomposed Ln-POT compounds and the linear extrapolation of the main absorption peak (O(p) → Ti(d) in the Ti_xO_y-framework). The X intercept is taken as an estimate of the band gap of the materials. Errors are estimated to be around ± 0.1 eV.

In order to compare the band gap results obtained from linear extrapolation of the UV-Vis absorbance spectra to the literature the data were analysed using a direct band gap semiconductor model (Tauc plots).[1] The results are summarised in Table S9.

Ln	HOMO-LUMO gap solid-state (eV)	Solid-state band gap (eV)
La	2.63	3.08
Ce	2.46	2.13
Nd	3.22	2.81
Sm	3.19	2.83
Eu	3.22	2.94
Gd	3.21	2.90
Tb	3.02	2.44
Dy	3.19	2.87
Ho	3.27	2.87
Er	3.22	2.77
Tm	-*	2.84
Yb	3.02	3.09

*not enough sample was obtained.

Table S9 HOMO-LUMO gaps for the molecular Ln-POTs in the solid state and band gaps of the decomposed materials (solid state) obtained from Tauc plots. Errors are estimated to be around ± 0.1 eV.

[1] Y. Lv, J. Cheng, P. D. Matthews, J. P. Holgado, J. Willkomm, M. Leskes, A. Steiner, D. Fenske, T. C. King, P. T. Wood, L. Gan, R. M. Lambert, D. S. Wright, *Dalton Trans.*, 2014, **43**, 8679

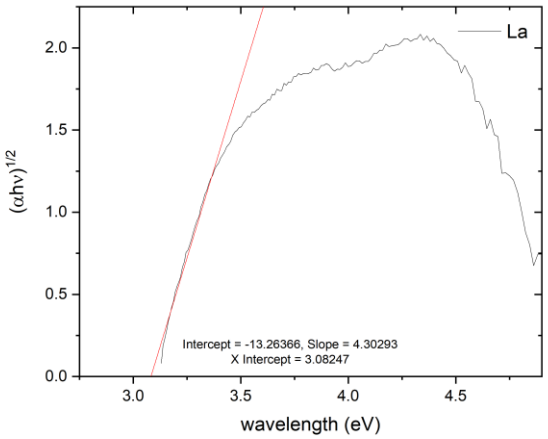
La
Intercept = -13.26366, Slope = 4.30293
X Intercept = 3.08247
(αhν)^1/2
wavelength (eV)

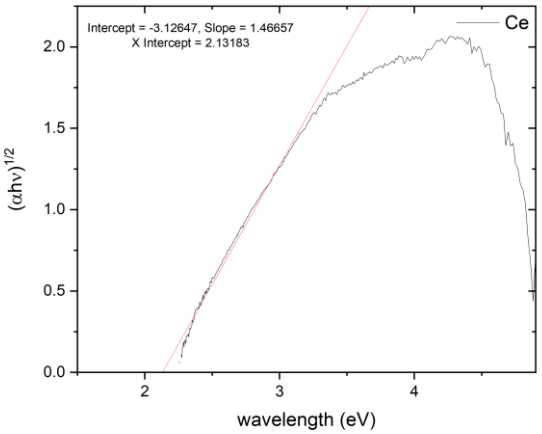
Ce
Intercept = -3.12647, Slope = 1.46657
X Intercept = 2.13183
(αhν)^1/2
wavelength (eV)

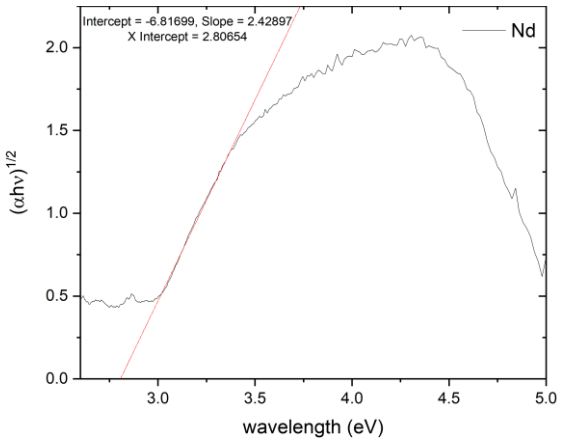
Nd
Intercept = -6.81699, Slope = 2.42897
X Intercept = 2.80654
(αhν)^1/2
wavelength (eV)

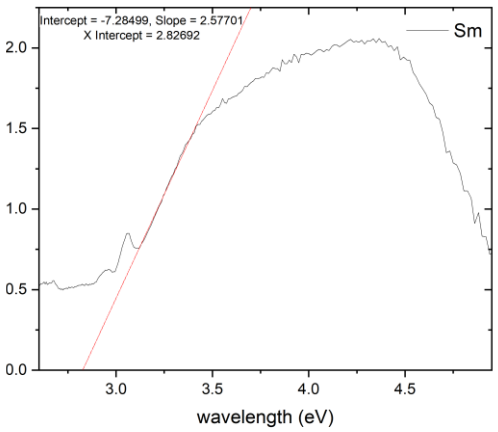
Sm
Intercept = -7.28499, Slope = 2.57701
X Intercept = 2.82692
(αhν)^1/2
wavelength (eV)

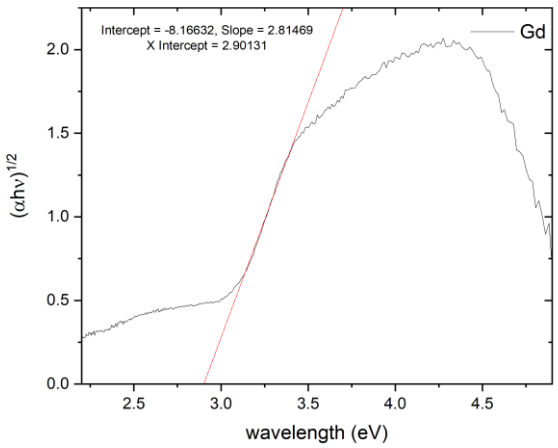
Gd
Intercept = -8.16632, Slope = 2.81469
X Intercept = 2.90131
(αhν)^1/2
wavelength (eV)

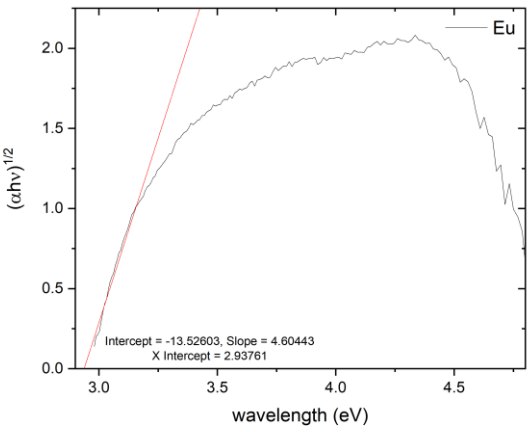
Eu
Intercept = -13.52603, Slope = 4.60443
X Intercept = 2.93761
(αhν)^1/2
wavelength (eV)

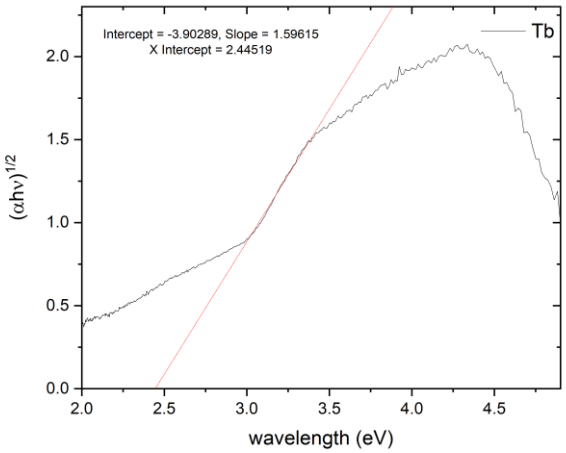
Tb
Intercept = -3.90289, Slope = 1.59615
X Intercept = 2.44519
(αhν)^1/2
wavelength (eV)

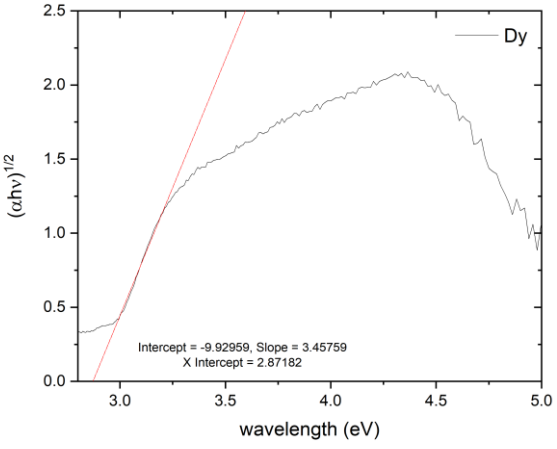
Dy
Intercept = -9.92959, Slope = 3.45759
X Intercept = 2.87182
(αhν)^1/2
wavelength (eV)

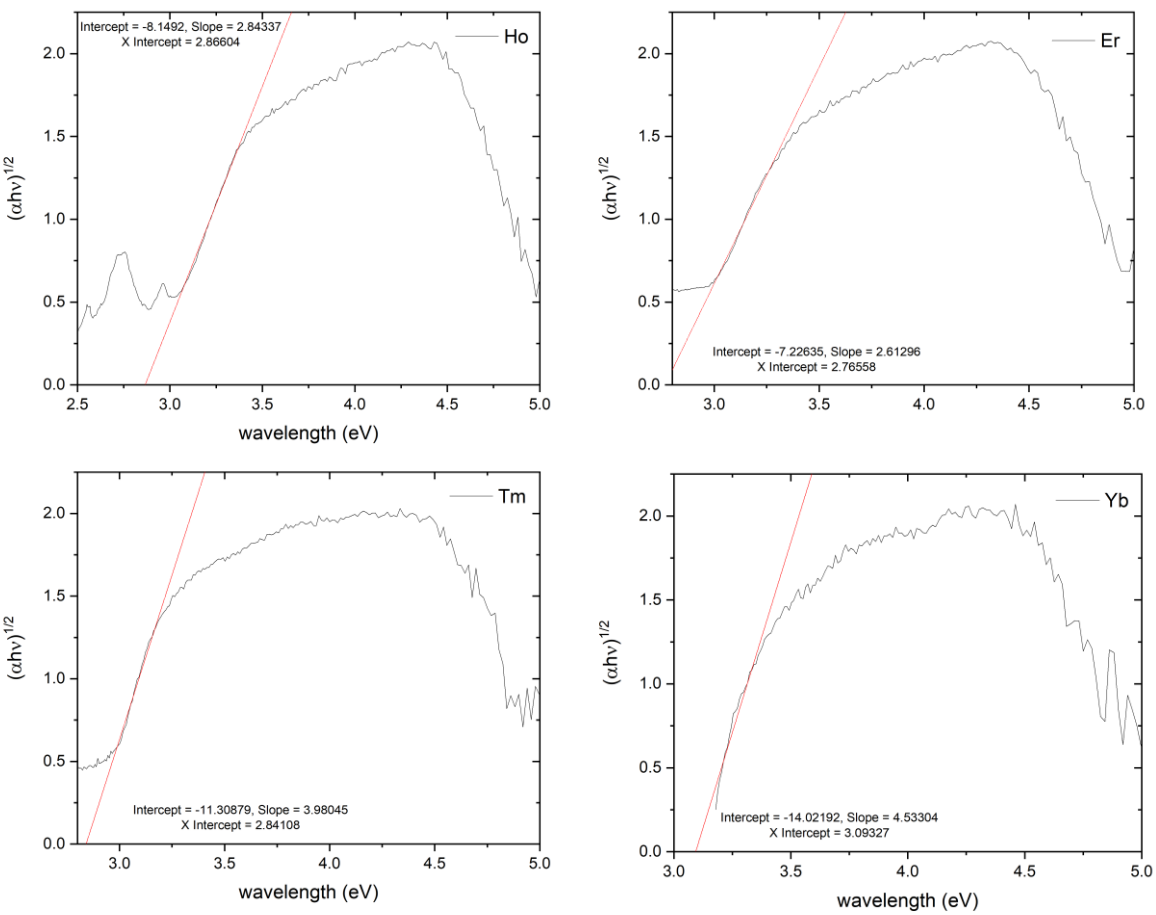

Figure S24 Band gap determination for the decomposed Ln-TiO_2 materials (solid state) using Tauc plots obtained from plotting $(\alpha h\nu)^{1/2}$ against the photon energy. Extrapolation of the linear section of the graphs gives the band gap E_g as the x-axis intercept. A similar analysis was carried out for the Ln-POT cages.